Beam shaping using Spatial Light Modulator

A dissertation submitted for the partial fulfilment of
BS-MS dual degree in Science

in

CHEMICAL SCIENCES

By

Dharm Singh Yadav

MS15112

Indian Institute of Science Education and Research Mohali
June 2020

CERTIFICATE OF EXAMINATION

This is to certify that the dissertation titled "**Beam shaping using Spatial Light Modulator"** submitted by **Mr. Dharm Singh Yadav** (Reg. No. MS15112) for the partial fulfilment of MS degree program of the Institute, has been examined by the thesis committee duly appointed by the Institute. The committee finds the work done by the candidate satisfactory and recommends that the report be accepted.

Dr. Jino George Dr. K.P. Singh Dr. Arijit Kumar De
(Supervisor)

Date: 30 June, 2020

DECLARATION

The work presented in this dissertation has been carried out by me under the guidance of Dr. Arijit Kumar De at the Indian Institute of Science Education and Research Mohali. This work has not been submitted in part or in full for a degree, a diploma, or a fellowship to any other university or institute. Whenever contributions of others are involved, every effort is made to indicate this clearly, with due acknowledgement of collaborative research and discussions. This thesis is a bonafide record of original work done by me and all sources listed within have been detailed in the bibliography.

Dharm Singh Yadav

(Candidate)

Date: 30 June, 2020

In my capacity as the supervisor of the candidate's project work, I certify that the above statements by the candidate are true to the best of my knowledge.

Dr. Arijit Kumar De

(Supervisor)

ACKNOWLEDGEMENTS

First of all, I would like to thank Dr. Arijit Kumar De, my project supervisor for his kind supervision and guidance. I have had this great experience and pleasure to work in his resourceful laboratory which provides great opportunities for me to improve both my academic and hands-on experience. He is also a kind and generous person who is willing to teach and share his knowledge and experience.

I would also like to thank Prof. J. Gowrishankar Director, IISER Mohali, Prof. Debi P Sarkar, former Director, IISER Mohali for providing a conducive environment which was very helpful for completing the thesis in time.

I would also like to express my appreciation to my committee members Dr. Jino George and Dr. K.P. Singh for the important discussions and valuable inputs to make this research accurate and comprehensive.

I would also like to give my special thanks to Dr. Anita Devi for providing her great advice and guidance in my dissertation study.I also deeply appreciate the help from Mr. Sumit and would like to thank him for his help in experiments, kindly guidance, and for his optics knowledge, without his dedication, this work would not have been possible.

I am very grateful to every lab member of the “Ultrafast Dynamics and Optical trapping” group who helped in my research, Dr. Arindam Das, Dr. Subhash Chander, Ms. Yogita Silori, Ms. Shaina Dhamija, Ms. Samita Mishra, Ms. Garima Bhutani, Ms. Sakshi Chawla, Ms. Umang Gupta, Mr. Subho Mitra, Ms. Dipali for their support, inspiration and fruitful discussions.

I wish to thank my friends fukrey for their support and encouragement throughout my study.

Furthermore, I am eternally grateful to my parents, Mr. Kailash Chandra Yadav, Mrs. Soni Devi for their love, care and support.

CONTENTS

LIST OF FIGURES

ABBREVIATIONS

CGH: Computer Generated Hologram

CMOS: Complementary Metal Oxide Semiconductor

DOE: Diffractive Optical Element

LC: Liquid Crystal

LC-SLM: liquid crystal spatial light modulator

LCOS: Liquid-Crystal on Silicon

LG: Laguerre Gaussian

OAM: Orbital Angular Momentum

SAM: Spin Angular Momentum

SLM: Spatial Light Modulator

HG: Hermite Gaussian

TN: Twisted Nematic

Abstract

Laser beam shaping is a process of redistribution of the irradiance and phase of optical radiation. By changing the irradiance and phase of the beam profile, we can also control the propagation of the laser beam. The optical beam control method is an important technique that is used in many different areas of research. The form of the laser beam usually corresponds to its irradiance profile, while the direction of the beam typically determines its propagation characteristics.

Here in this thesis, we have presented both theoretically as well as experimentally the transformation of a Gaussian beam into a Laguerre Gaussian (LG) and Bessel beams by a phase-only liquid crystal spatial light modulator (LC-SLM) is based on the reflective beam shaping method. Where Computer-generated holograms can be used for shaping millimetre-wave beams and for producing complex field configurations. In accordance with the theory of energy conservation and constant optical path, the phase distribution can properly modulate the wave-front to generate the LG and Bessel beam. We have successfully generated the LG and Bessel beams and verified it with the interferometric setup using plane wave and spherical wave propagation as a reference beam. Our results are in nice agreement with the theoretical results.

Chapter 1

Introduction

1.1 Brief History

The beam shaping dates back to the seventh century B.C, a long, interesting and controversial history, when people used magnifying glasses to direct sunlight on wood to ignite them [1]. The use of solar energy for heating, cooling and electricity production has been an ongoing interest [2]. Early thoughts of beam formation can be traced back to before the days of Archimedes and his burning glass [3, 4] when the application of optics was stated to maximize solar energy efficiency. The literature includes reports from a ranging number of optical systems in use as solar collectors [5-9]. Welford, and Winston have shown that non-imaging (non-focusing) optics used as solar collectors are well accounted for, including an ideal light collector [11, 12]. The differential equation approach was used by Burkhard and Shealy [13] to design a reflecting surface, which distributes the irradiance over the receiver surface. McDermit and Horton [14, 15] introduced a general technique for the design of a rotating symmetrical reflecting solar collector to allow the collector surface to be heated in a prescribed way. Beam shaping has also been used in opto-electronics to achieve maximum power transfer between a micro-optics light source and an optical fiber [16, 17] in radiative heat transfer [18-20] in illumination applications [21-24] and for reflector synthesis. [25, 26]. It is very important that the target surface is uniformly illuminated for light applications with a laser beam, for example in holography, material processing and lithography. Optical devices were used to shape laser beam intensity profiles, based on reflective [14, 28, 29] and refractive [30-34] optical systems. McDermit and Horton also made a prescription for using a non-uniform input beam profile to use energy conservation within a bundle of rays to design rotationally symmetric optical reflection systems for illuminating a receiving surface. Two mirrors laser profile shaping system with rectangular symmetry was been designed by Malyak, Shealy and Chao [29]. In order to achieve a desired output intensity distribution and wave front shape, Kreuser [29] patented a consistent light optical System with the use of two aspherical surfaces. In order to calculate the form of two-aspherical surfaces on the lens system expands and converts the laser profile of the Gaussain to a collimated, uniform radiation beam, Rhodes and Shealy [32] derived the use of intensity and constantly optic path length conditions for differential equations. Two plano-aspherical lenses were designed, manufactured and used in the holographic projection system for laser beam shaping using their methods [35-37]. Hoffnagle and Jefferson [34] then introduced aspherical convex surfaces in order to make the output beam profile formation easy and continuously roll off of the output beam profile

to control the patterns of the remote diffraction in their design of the system to form a refractive laser beam. From early work by Frieden [30] and Kreuzer [31] in the 1960s, the optical construction of laser beam shaping systems has evolved considerably to the contemporary work of many of them [38-40]. Recent research has well expressed the aims of some technologies to shape the laser beams. Peace and Kreuzer tried to establish an optical system that would transform an input plane wave with a Gaussian irradiation profile into a uniform radiation output plane wave. For non-linear mapping of ray coordinates between input and output planes, the conservation of the energy over a bundle of rays was used. Frieden also showed that, after redistribution of radiation, the stage of the beam across the output plane will differ by 20λ.Thus, a second optical element must correct the phase distortions imported through irradiance redistribution for laser beam shaping applications when the output beam phase is important. The shape of aspheric surface refracting, which re-collimate the output beam parallel to the optical and input beams, was calculated by Frieden. Of all rays that travel through the beam forming optics, Keuzer has set the constant optical path length condition to monitor variance of the output beam. Unfortunately, optical design and manufacturing technologies had not been sufficient until the 1980's for realistic laser beam shaping design, analysis, manufacturing and testing.

1.1.1 Methods of beam shaping

Today, generally we define beam shaping as the process of redistribution of the irradiance and phase of a beam of optical radiation. The output beam phase determines the propagation of the beam. The general problem of beam shaping is shown in figure 1.1. An optical system consisting of one or more elements, collectively used to modulated the input beam in to desired output beam. To generate the desired power, the optical system must operate on the beam. The designed optical system may or may not be used to restrict the beam phase of the input coherent beams. For example, the phase front of the beam coming out of the optical device has to be standardized if a collimated beam of output is needed. If only a certain radiance distribution at the target plane is required then in that case the design of the optical system is usually simpler as the phase remains uncontrollable. Phase considerations apply to incoherent beams and the correct distribution of irradiation is then taken into account. So the choice of beam shaping element to be used depends upon the requirement of the output beam.

Laser beam shaping is the way in which light beam amplitude and phase are redistributed using a certain optical element. The type of beam is defined by the irradiance profile and

propagation properties of the profile of the beam. Laser material processing research, laser arms, optical data, image processing, lithography pattern, printing, and laser art are among the applications of beam shaping [41].

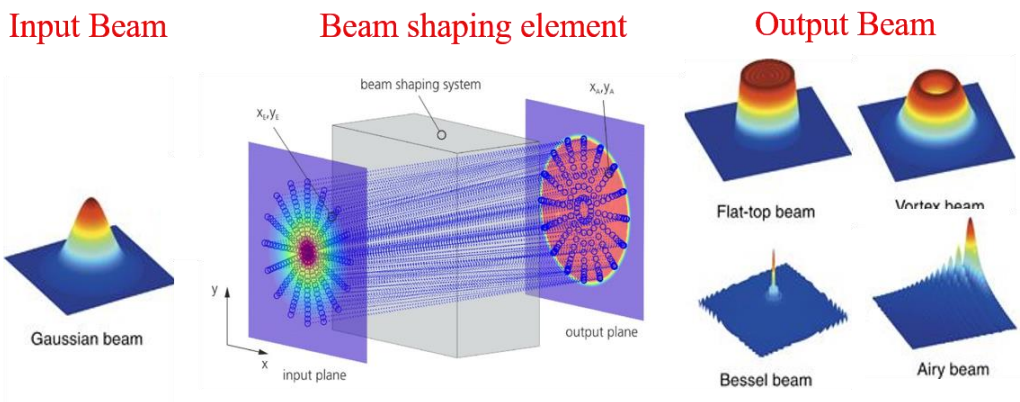

Figure 1.1: Schematic diagram of the redistribution of rays to generate various beams out of Gaussian intensity distribution [42].

Contemporary laser beam shaping systems can be grouped into three broad functional categories:

1. Beam Aperturing: This is the trivial, very ancient, method of the beam shaping, the schematic of the beam shaping system used in this method is shown in figure 1.2. In this method, the beam is expanded and an aperture is used to select a suitably flat portion of the beam. Magnification of the resultant irradiance pattern is calibrated to change the output beam size. The biggest downside to this approach is that much power or energy from the incoming beam is lost. Since, it important that the beam shaping operation should conserve energy, which leads to ineffectiveness of this method for many applications. Furthermore, if the radiation of the input beam is not smooth, an appropriate aperture and position which is required to get the desired outcome may not be found. The aperturing of the beam is illustrated in figure 1.2. In this case, the beam is expanded and an aperture is used to select a suitably flat portion of the beam [43].

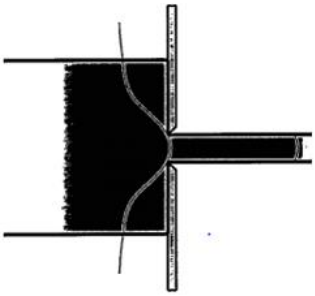

Figure 1.2: Uniform irradiance obtained by aperturing input beam.

2. Field Mapping: The mapping of field is most basic amongst all the available beam shaping methods. Field mapping is characterized as the design of a number of optical parts that map a specified optical field into a desired optical output field. In this method, only a given or limited magnitude of the optic field output is constrained or modulated. A field mapper converts a common input beam into a prescribed output beam, essentially lossless and works well for single mode beams. Field mappers transform the input field into the desired field in a controlled manner. The basic field mapper concept is illustrated in figure 1.3 for the case of mapping a single-mode Gaussian beam into a beam with a uniform irradiance [43].

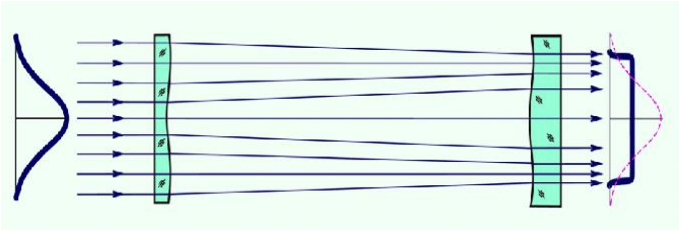

Figure 1.3: Field mapping schematic diagram.

In figure 1.3, Gaussian distributed rays are bent in a plane so that they are uniformly distributed in the output plane. The ray bending defines a wave-front that can be associated with an optical phase element. Field mappers can be made effectively lossless. The field mapping approach to beam shaping applies to well define single-mode laser beams. But again, this method is also limited because the optical component used to do shaping needs to vary according to the requirement.

3. Beam integrator: It normally splits the incoming beam into a wide variety of facets with a lens variety and attempts to distribute the energy through the output area of each facet. The output beam profile is a measure of each lens array aperture's diffraction pattern. This method works very well in case of multimode beams [42].

The physical or geometrical optics can be used for constructing the beam shaping systems. However, there is no single method of beam shaping that can be employed for all kind of applications. A parameter is defined which helps in choosing a beam shaping technique. The measurement of parameter β will help to assess the quality of the available solution and whether the methods of geometric or physical optics should be employed [44].

$$\beta = \frac{2\sqrt{2\pi}}{f\lambda} r_0 Y_0 \qquad (1.1)$$

where λ is the wavelength, r_0 is the beam radius or waist, Y_0 is half-width of the desired output dimension, and f is the focal length of the focusing optic, or the working distance from the optical system to the target plane for systems without a defined focusing optics.

• For $\beta < 4$, beam shaping system may not produce acceptable results.

• For $4 < \beta < 32$, diffraction effects become significant and should be part of design of beam shaping systems.

• For $\beta > 32$, geometrical methods should be adequate for design of beam shaping systems.

The above discussed beam shaping methods the efficiency of laser processing, but have problems with precision and flexibility. Therefore, we need a more flexible and precise method for beam forming which is therefore ideal for our study. In this thesis a novel method of beam shaping is illustrated and tested for the LG beam Bessel beam generation with accuracy. Modern SLM-based beam shaping techniques have serious advantages like it offers a uniform laser beam intensity distribution, better predictability and reliability, greater efficiency in the use of laser energy, simpler mathematical description of diffraction transformations, etc. The key benefits of SLM is its ability to achieve beam modulation without mechanical moving parts combined with the maximum use of laser energy and a high capacity.

1.2 Spatial Light Modulator (SLM)

SLM is a powerful instrument based on LC technology, which is employed for both phase modulation and amplitude modulation of the input beam. In the beginning of the 1980s they were used in optical computing [45], SLMs are very popular in different field of research, including beam shaping [46, 47], correction of wave-front [48] and laser parallel processing [49]. SLMs are mainly divided into two classes: SLM which are addressed electrically and SLM which are addressed optically. For later case, a light encoded in the front or back of an image is used to construct and change the image. The SLM has the ability to sense the brightness of each pixel through a photo sensor and reproduce the image with the help of LC. In this experimental work of thesis, we have used a LC on silicon chip spatial light modulator (LCOS-SLM), it consists of a sheet of birefringent LC that is sandwiched between the electrodes. Each of the electrodes is pixelated, and the HDMI controller controls every pixel of the electrode according to the phase implemented by computer-generated hologram (CGH) [50]. The potential difference produced between these electrodes gives the LCs a tilt, and as the light passes through the crystals, there is a

phase delay that comes in the light beam. The driver adjusts the potential on the pixels according to certain discrete values between 0 and 255 which correspond to the phase delay from 0 to 2π.

Each pixel is driven independently by an accurate voltage controlled by the grey scale of the images. The image is considered as a matrix of the order of resolution as of SLM screen. The LC molecules rotate at a particular angle when they are provided with an external voltage, resulting in a change in the refractive index. Thus, the phase and polarization of input light after reflection gets modulated. Using the software, we write the phase in terms of a matrix and then save it as an image and then implement it on SLM which will be addressed briefly in chapter 2.

1.2.1 Working Principle

Liquid crystal on silicon (LCOS) technology for image and video display applications has been known for many years. This technology incorporates the distinctive light-modulating characteristics of LC and advantages of the high-performance silicon complementary metal oxide semiconductor (CMOS) technology through advanced LCOS mounting processes. In comparison to traditional LC displays, the LCOS can be either reflective or transmissive and enables the use of electrically modulation of optical properties in LCs to change the polarization or the direction of an incident light beam [51].

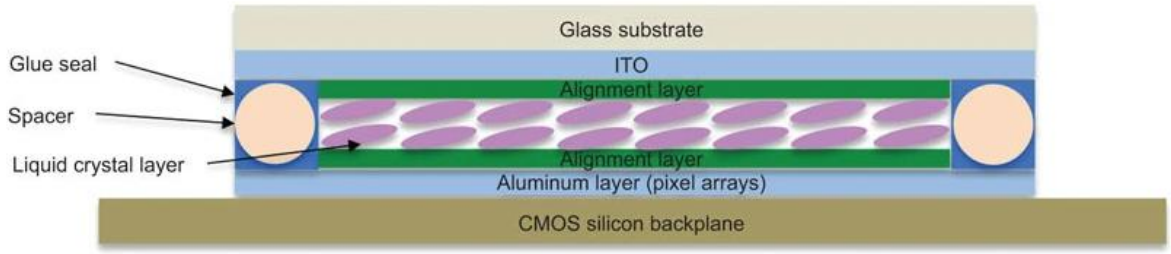

Figure 1.4: Schematic of phase-only LCOS devices.

LC SLMs are used for modulation of both intensity and phase. The Birefringence property is denoted as: They are transparent molecules in rod form which similarly align with crystals but can flow over each other like fluids. The molecules are randomly oriented in the nematic array, as used for SLMs, but can be aligned in a direction with an applied external electric field. Birefringence, which means they have a different refractive index perpendicular (n_o) and parallel (n_e) to the optical axis is another important property of LC, as shown in figure 1.5. The property of Birefringence is described as [51]:

$$\Delta n = n_e - n_o \tag{1.2}$$

Such molecules have an electric field orientation, and an applied electric field can rotate the optical axis. This allows for the slowing of the light between $[n_o - 1]c$ and $[n_e - 1]c$ across an LC layer, causing a delay in phase. Here, c is the velocity of light, n_o refractive index along the ordinary axis and n_e refractive index along the extra-ordinary axis.

As it can be seen in figure 1.6, most LCs have a rod shape. They are birefringent and have different relative axial and transverse dielectric constants, and thus different refractive indices. The temperature difference between the melting point and the clearing point, where the individual molecules are randomly distributed, is called mesophase.

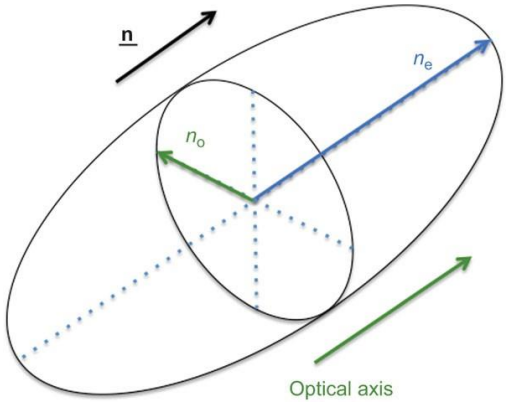

Figure 1.5: Spontaneous axis system inside a nematic LC, in which birefringence is equivalent to $n_e - n_o$ and is a function of the voltage supplied [51].

In an SLM case, LC material is normally sandwiched between two glass plates, forming a layer that is several microns thick. The LC substrates are protected by transparent electrode layers accompanied by orientation layers containing grooves pulling the neighbouring LC molecules to a particular alignment.

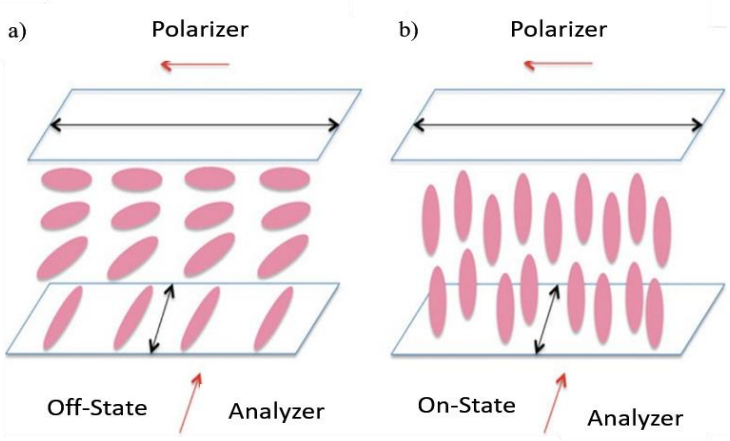

Figure 1.6: A schematic LC layer: (a) no external electric field and (b) as aligned by an external electric field normal to the LC layer [51].

As shown in figure1.4, the molecules are arranged in a Twisted Nematic (TN) LC layer. The molecules are a sort of helix (left picture) that is 'relaxed' (no voltage between the electrode layers). This form arises from the top and bottom layers of the perpendicular grooves. The p-type crystals are lined up with an alternating voltage between the electrode layers in the electric field. The frequency should be high enough to avoid relaxing the molecules. The flickering of lights, however, is always a concern with TN SLMs.

LCOS device architecture is identical to traditional LC devices except that one of the substrates as shown in figure 1.4 is a silicon backplane. The CMOS silicon backplane consists of an electronic circuit buried below pixel arrays which gives you a high filling factor. The pixels are reflections of aluminium mounted on the background surface of the silicon. With almost zero absorption, the incident light is transmitted through the LC layer. Integration of high-performance driving circuits allows the voltage on each pixel to be adjusted to monitor the phase delay of incident light across the device. LCOS system provides two types of light modulation, amplitude modulation, and phase modulation [51].

1.2.1.1 Amplitude modulation

In their initial implementation areas, TN microdevices were used as amplitude modulators, for example, back-projection television or screen projection. If the voltage of the cell is 0, and the thickness d of the LC layer satisfies the condition [52].

$$d = \sqrt{\frac{3}{2}}\left(\frac{\lambda}{\Delta n}\right) \tag{1.3}$$

Where λ is the wavelength of light, $\Delta n = n_e - n_0$, depicts the difference between the refractive indices in the axial and traverse direction of the LC molecules as shown in figure 1.5. The polarization of an incoming light beam polarized parallel to the operator of the first LC molecules is rotated approximately 90^0 after entering the entire LC cell as shown in figure 1.6. That is because of LC birefringence. When electrodes receive an alternating voltage, they arrange in parallel to the applied electric field, forming a homeotropic state which has no optical activity [53].The tilt angle (angle between the substrates operator and the plane) of the molecules is somewhere between 0^0 and 90^0 when the smaller voltage has been applied. In practice, a true modulation of polarization cannot be achieved by using a TN screen, i.e. without a coexisting phase modulation at least small. This mode of use is also often referred to as modulation of amplitude only.

1.2.1.2 Phase modulation

The phase manipulation of incident light using LCOS-SLM, is achieved by the birefringence of the LCs, which is the principal material property of these crystals. The phase delay is obtained by adjusting the refractive index along the light path electrically. In LCOS-SLM device, the tilt directions of the alignment layers of both glass substrates are perpendicular to each other as shown in figure 1.6, and the LC molecules achieve a 90° twist across the LC cell [51]. The strong interaction between LC molecules and the subtract surface can regulate the re-orientation of the LC with the help of an external electric field. Due to the optical birefringence property of the LCs, the effective optical refraction coefficient varies accordingly and create a phase retardation which is regulated with the help of external applied voltage.

In this thesis, we explore the significance of SLM in laser beam shaping as a phase modulator for the adaptability of a wide variety of beam designs and to produce non-diffractive laser beams. The thesis offers explanations of how Laser beam shaping is supported by SLMs. Through this work, we demonstrate the use of an SLM to create beams with different transformation characteristics and define the processes as well as the experimental results. Here we introduced theory of beam shaping and experimental implementations using 1920×1152 reflective SLM from Meadowlark optics shown in figure 1.7.

Figure 1.7: LCOS-SLM from Meadowlark optics
(Taken from https://www.meadowlark.com/).

It reveals what it is made of, and how it modulates the field of light. The theory is discussed in relation to diffractive optics, the Huygens-Fresnel principle is used to define diffraction

in terms of amplitude and phase of the light field and the two approximations resulting in Fresnel and Fraunhofer diffraction integrals. Diffraction theory is used to explain a simple lens structure, and those equations are applied to the pixelated SLM

Chapter 2

Theoretical Studies

2.1 Introduction

2.1.1 Laguerre Gaussian beams

It is well known that light carries momentum that is of two types that is linear momentum and angular momentum. Depending on the type of beam, we can get to know the type of momentum carried by the beam. For example, the Gaussian beam carries linear momentum, however, the LG beam carries angular momentum which further characterizes into orbital angular momentum (OAM) and spin angular momentum (SAM). While the SAM is known to refer to the polarization of the (light) beam, the OAM characterizes the spatial field distribution and the formation of helical wave-fronts. Because of their helical phase fronts, these beams are also often referred to as twisted beams. In both contexts, light holds a portion of momentum that is not parallel to the direction of propagation of the light [54]. We are particularly interested in the collection of modes defined as the LG modes in this thesis. Two indices that describe the electric field of the LG mode are 'p' and 'l' these are known as radial and azimuthal index respectively. Here we have explored the LG modes for the different l and p indices. The index 'l' can take any integer value. Figure 2.1 depicts the simulated intensity patterns of a Gaussian beam and a LG beam with l = 1.

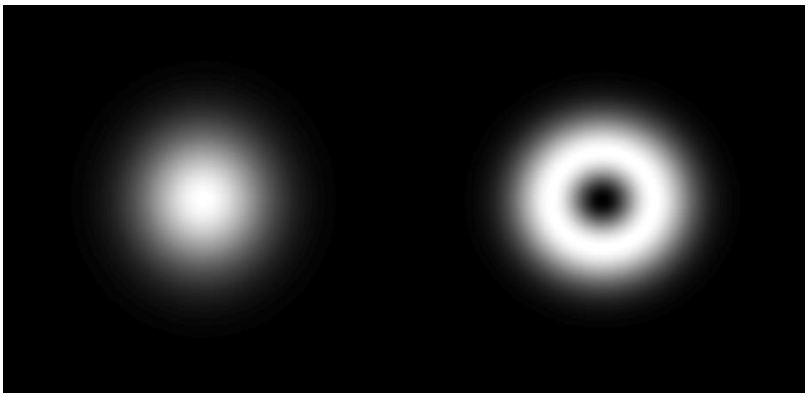

Figure 2.1: Simulated intensity profile of Gaussian (left) and LG mode with l = 1 (right).

Although this intensity plot hides the complexity of the LG modes. For electromagnetic radiation, the Poynting vector characterizes the direction and extent of the energy transfer. The Poynting vector points along the beam direction, in the simple Gaussian light beam. By comparison, in the LG modes, the Poynting vector travels along with the coil as the beam propagates. The index value l is indicative of the tightness of the spiral of the Poynting vectors.

There are many different ways to create a beam in a LG mode. One approach requires placing the laser beam across two π/2 mode converters. However, this approach demands the input also be one of the Hermite-Gaussian (HG) modes. Each HG mode is transformed into another LG mode. The recommended approach in this analysis is one that uses an SLM to create different LG modes from a simple Gaussian beam by implementing computer-generated hologram generated using Matlab (Mathworks R2018a) onto the active region. The simulated grating is shown below in figure 2.2.

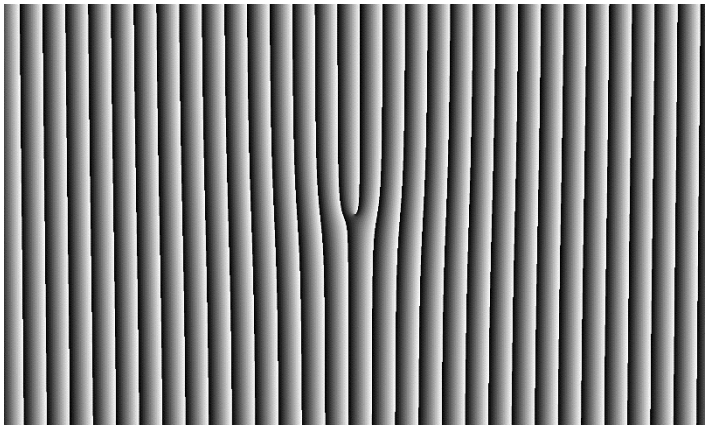

Figure 2.2: A simulated forked diffraction grating for l = 1.

The diffraction grating is shown in figure 2.2 for l = 1, implying that if this grating is illuminated with a Gaussian beam the very first order diffracted beam would be the l = 1 LG mode at the first order of diffraction. Besides, the diffracted beam of the mth order will be in l = m mode of LG. The mathematical basis of these forked grating is to be further discussed in this chapter.

The most interesting thing about the LG modes is that they carrying OAM. A light beam in LG mode with index l has an OAM $l\hbar$ per photon. Since l only can take integer numbers, the OAM is quantized [55]. The fact that l can only take integer values follows from an exponential $e^{il\varphi}$, a term in the electric field amplitude of the LG modes (here, φ is the angle in the plane perpendicular to the beam axis). As we expect, this term oscillates about the beam axis with a frequency corresponding to l. Of course, if φ is increased by 2π, then the field should be the same. In other words,

$$e^{il\varphi} = e^{il(\varphi+2\pi)} = e^{il\varphi}e^{il2\pi} \tag{2.1}$$

Here, $e^{il2\pi}$ will equal 1 only if l is an integer. Thus, the OAM is quantized for beams with φ dependence $e^{il\varphi}$ [56].

The OAM variable exhibits quantum properties very similar to those of the spin variable for photons. It has been shown experimentally that pairs of photons can be entangled in OAM [57]. The variable l can take on any integer value. Also, there are strong classical reasons to believe that the quantum states which correspond to the LG modes have a complete and orthogonal basis [58]. In other terms, OAM of a photon can also be defined as a linear arrangement of LG states but none of the LG states itself can be defined as a linear combination of any other LG states. For this reason, LG states define an infinite-dimensional Hilbert space [55].

The study of the quantum properties of the LG states is a hot topic, especially, studying the entanglement properties. But in order to perform entanglement experiments, we must first have a solid understanding of how the LG modes can be generated, superimposed, and sorted efficiently. In this chapter, we have aimed to familiarize the reader with the fundamentals of LG beams that will be helpful in subsequent chapters. However, the structure of light has always been a constant thread throughout my research, it is much too large a topic to be discussed in its entirety. We have confined ourselves to basic explanations and avoid overly complicated mathematical models.

2.1.2 Bessel beams

Diffraction is an edge point in optics that has applications for the construction of optical networks. Here we have talked about a type known as “non-diffracting light” [59]. Usually referred to as Bessel beams. Estimates of these beams can always be achieved experimentally by a lot of methods. The theoretical background of this type of beam is discussed and then several experiments using these beams are explained: which include a broad variety of areas involving non-linear optics, optical tweezers etc. The Bessel beam has property of intense center, which has drawn interest in areas including atomic optics, where the Bessel beam's contracted non-diffracting property may behave like an atom guide, also in confinement systems and optical engineering, in which the beam's regeneration characteristics help to detect new results which cannot be seen with Gaussian beams. Diffraction is indeed an exquisitely related process of a wave property of light that happens if a wave meets an object. The wave-front portions propagating across the obstruction intervene in a certain fashion and produce a sequence of diffraction. By fact, a laser intensity is considered to be "pencil-like" and generally, the divergence is also minor but laser light can be easily subjected to diffraction which enables the beam scattering. The light can be controlled in order to create a collimated beam or a tightly focused beam relying

on the act of concern. Rayleigh limit z_R is the standard factor that is used to describe the expansion of a Gaussian beam and represents the range in which doubling of the cross-section of the Gaussian beam takes place.

$$z_R = \frac{\pi w_0^2}{\lambda} \tag{2.2}$$

here, λ and w_0 represents the wavelength and beam waist width respectively. From the perspective of various uses including medical imaging and atom optics, the idea of resolving diffraction has always been strongly plausible and also tempting. This thesis tries to deal with the generation of the Bessel light beam. Durnin *et al.* had first reported the Bessel beams as a mathematical model [60]. They focused on Whitaker's Helmholtz equation solutions and found that similar Bessel-like solutions were irrespective of the direction of propagation. These beams use a Bessel function of the first kind, Bessel term comes from the definition of this kind of beam, and this contributes to an extrapolated profile cross-section of concentric rings. Mathematically these beams should spread large power across an infinite field since they have an infinite number of rings. They also showed only that one could experimentally effectively estimate something like a Bessel beam that holds the mathematical body's characteristics over a limited area. At first, the idea of any "non-diffracting" beam appeared quite controversial and indeed remained so, the previous study claims that the Bessel beam was often only a line pattern and it was not exceptionally new since it was just somewhat close to Poisson's spot only [61]. However, later the same group explained that there can also be several ways of producing these type of line patterns and they won't need to illustrate characteristics of Bessel beam. It was also verified, as the group figured out in their response, that there are beams for whom central peak is strikingly insensitive to the diffraction usually associated with all wave propagation [62].

2.1.2.1 Properties of Bessel beam

One can define the electric field of a perfect Bessel beam by:

$$E(r, \varphi, z) = A_0 e^{ik_z z} J_n(k_r r) e^{\pm in\varphi} \tag{2.3}$$

In which J_n is termed as Bessel function. Also, k_z and k_r represent the longitudinal and radial wave vectors respectively, in which $k = \sqrt{{k_r}^2 + {k_z}^2} = \frac{2\pi}{\lambda}$. Parameters, z, r, and φ are the longitudinal, radial, and azimuthal components [63]. Figure 2.3 indicates the

intensity pattern of the zeroth-order and the first-order Bessel beam. Bessel beams with higher-order are defined by Bessel functions J_n (where n > 0), these higher orders have a singularity in the phase on the axis of the beam. Therefore, the consideration concludes that the solution obtained for the Helmholtz equation follows the equality, where the intensity, I, obeys the following relation of propagation [64].

$$I(x, y, z > 0) = I(x, y) \tag{2.4}$$

It, therefore, makes it more likely to assume that indeed the beam is free from diffraction and remains invariable during propagation as well since when the light propagates there is no shift in the cross-section. Another method or way to understand this kind of beam is to consider a collection of plane waves that are propagating on the surface of a cone. Every propagating wave is subjected to a similar phase change, $k_z\Delta_z$ throughout a distance of Δ_z. Such a breakdown of the Bessel beam using planar waves expresses within the angular spectrum of the beam, which is a kind of a loop or a ring-type structure in k-space. Therefore, the optical Fourier transformation of this loop would result in a Bessel light, and that is how Durnin *et al.* found the first experimentally approximation to a Bessel beam [60]. The beam's description into plane waves indeed provides a means of characterizing a Bessel beam that of the cone's opening angle θ, is described with the help of the waves which traverse its surface. The expression for this is given below:

$$\theta = tan^{-1}\frac{k_r}{k_z} \tag{2.5}$$

Also, the beam's central spot dimensions given by: $r_0 = \frac{2.405}{k_r}$.

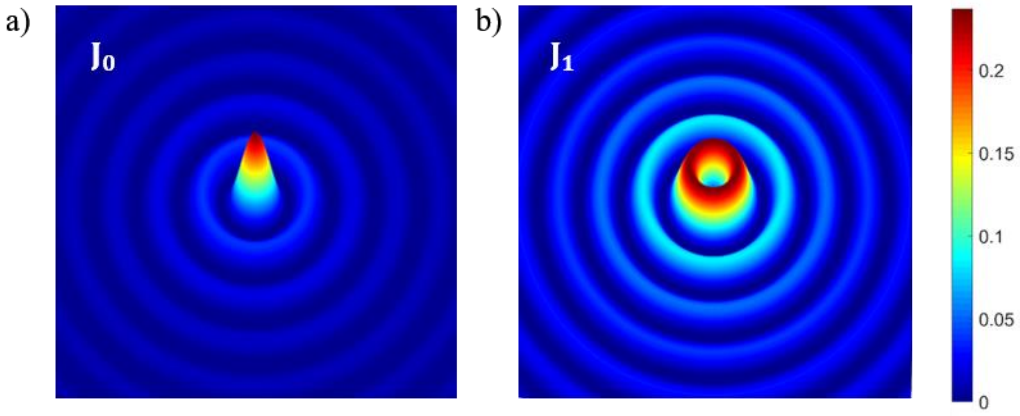

Figure 2.3. Illustration for Bessel beam intensities: (a) zeroth-order mode and (b) first-order mode

It is essential to keep in mind that perhaps the Bessel beam has a unique property that the energy (or power) is equally distributed among all of its rings, so the lower the energy in

the central part of the cone, more is the number of rings the beam will have. This property is advantageous in certain experimental cases because if we have a higher number of rings, it results into enhancement in the propagation length. Durnin *et al.* has also demonstrated and proved that the above assumption did not imply that a Bessel light could not carry power effectively like a Gaussian beam like one might believe naively to do [60]. Nevertheless, modified Gaussian beams and Bessel beams are found to be comparatively more effective at transferring power. They have also demonstrated that one can manage the beam's depth of field for the Bessel beam and can be made even more significant than that of the Gaussian beam but it might result in power loss in the central region.

It was also showed that the beam nodes directly relate to a π phase change between neighbouring rings, which leads to the idea that a Bessel beam can also be assumed to be consisting of a number of the plane waves propagating on the surface of cone. A Bessel beam creation is achieved in a variety of different way. The Bessel beam can be considered as a Fourier transformation of a round ring. This beam however, can also be generated using an aspect of the conical lens or an axicon [63]. The use of an axicon is much more useful than that of the slit which is annular because this axicon generally uses the entire or sometimes a small part of the input beam. The advantage of using axicon for Bessel beam generation is the elimination of the intensity fluctuation, which cannot be neglected during the process done with annular slit, which results in a much smoother variance in intensity. The alignment of the axicon with the input beam is crucial in generating a Bessel beam. Every oblique lighting lead to the introduction of an aspect of astigmatism and this leads to a sequence form like a chequerboard rather than a location on axis with a series of circles lying in a concentric manner. Other effective techniques of generating Bessel beams exist, such as the use of holographic methods that imprint a suitable phase required for Bessel beam generation on the Gaussian input beam. However, the modern method for Bessel beam generation involves the creation of the holograms; or adjustable holograms created with software-operated tools like SLM that we have discussed in much more detail in the next section.

2.2 Theory of generation of CGHs

To look deep insight how the forked diffraction gratings are created (described in section 2.1.1) to convert a Gaussian laser beam to a Laguerre-Gaussian beam, first, it is necessary to understand a few basic principles of holography. In a general sense, a hologram is like a photograph in that optical information is stored. Unlike a photograph, however, a hologram stores information about both the intensity and the phase of the field of the object [64], basic diagram of how a hologram works are shown in figure 2.4.

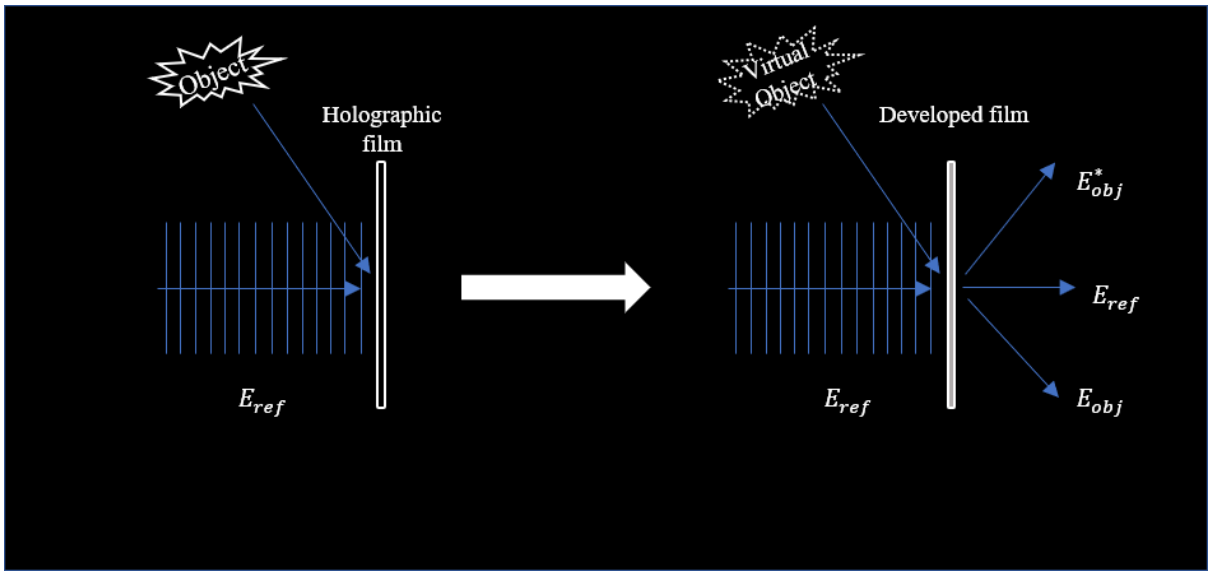

Figure 2.4: Simplified depiction of working of hologram.

When the hologram is being formed, there is the interference of the reference beam with the light from the object that we are trying to image as depicted as a plane wave in figure 2.1. The interference pattern formed by the reference wave and the object wave is what recorded on the hologram. So, if the reference wave is described by E_{ref} and the object wave by E_{obj} the intensity recorded on the hologram is given by the following equation:

$$I = |E_{ref} + E_{obj}|^2 = E_{ref}^2 + E_{obj}^2 + 2Re[E_{ref}E_{obj}^*] \quad (2.6)$$

The first two terms relate to the corresponding intensities of both the source beam and the reference beam. The final term is that it includes details of the two beams' relative stages. The way we have retrieved the information is illustrated in figure 2.4. When the SLM is illuminated with the reference wave, an exact copy of the object wave is obtained as the output on the other side of the hologram at the angle (relative to the reference wave) at which it was input. There is also a beam output at the opposite angle which is the complex

conjugate of the object beam, and a transmitted beam that has the same form as the reference.

What we wanted to do in the context of this experiment is the image of a mode of laser light rather than an object. Since we do not have the mode we are interested in, to begin with, it is easiest to generate the necessary holograms using a computer. For reference, here is the spatial amplitude distribution of an LG mode with azimuthal index l [65]:

$$u_l(\mathrm{r},\varphi,\mathrm{z}) = \frac{C_l^{LG}}{w(z)}\left(\frac{r\sqrt{2}}{w(z)}\right)^{|l|}\exp\left(-\frac{r^2}{w^2(z)}\right)L_0^{|l|}\left(\frac{2r^2}{w^2(z)}\right)\exp\left(\frac{r^2}{2(z^2+z_R^2)}\right)\times$$
$$\exp(\mathrm{il}\varphi)\,exp\left(\mathrm{i}(|l|+1)arctan\left(\frac{z}{z_R}\right)\right)\exp\,(ikz) \qquad (2.7)$$

here, beam waist, w(z) is given by:

$$w(z) = w(0)\sqrt{1+\frac{z^2}{z_R^2}} \qquad (2.8)$$

Where, z_R (Rayleigh range) and $L_0^{|l|}$ is generalized Laguerre polynomial which is given by:

$$L_0^{|l|}(\mathrm{x}) = \frac{e^x}{x^{|l|}}\frac{d}{dx}\left(e^{-x}x^{|l|}\right) \qquad (2.9)$$

We simulated the interference of l = 1, LG beam coming at an angle with a Gaussian reference beam as shown in figure 2.4. Figure 2.5 shows the simulated interference pattern which looks like a forked diffraction grating.

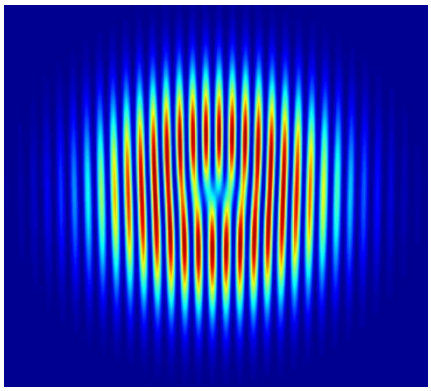

Figure 2.5: Simulated interference of LG beam and Gaussian reference beam.

As it turns out, this analysis is slightly overcomplicated for our purposes. The vital difference between a Gaussian beam and a LG beam is the phase $e^{il\emptyset}$. At the most fundamental level, all we did is, imparted a phase $e^{il\emptyset}$ onto a beam that has a tilt-in, say, the x-direction. In other words, the object beam has a phase $e^{il\emptyset}$ relative to the reference beam and the reference beam has a phase e^{ikx} relative to the object beam. The intensity profile of this simplified hologram is then given by equation 2.10 [66]:

$$\mathrm{I(x,y)} = \left|\mathrm{e^{ikx}} + \mathrm{e^{il\varphi}}\right| = 2 + 2\cos(\mathrm{kx} - l\varphi) = 2 + 2\cos\left(kx - l tan^{-1}\left(\frac{y}{x}\right)\right) \quad (2.10)$$

In the above equation, $|l|$ varies the number of dislocations in the forked pattern, the sign of l varies whether the pattern is oriented upright or inverted, and k_x varies the spacing of the fringes. A few holograms created with this intensity profile are shown in figure 2.6.

$$(\mathrm{e^{il\varphi}})^* = \mathrm{e^{-il\varphi}} = \mathrm{e^{i(-\,l)\varphi}} \quad (2.11)$$

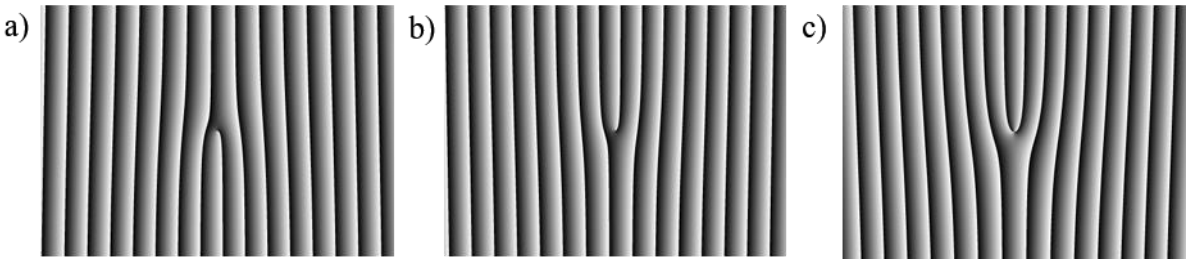

Figure 2.6: Simulated greyscale fork diffraction grating; (a) $l = -1$, (b) $l = +1$, and (c) $l = +2$.

2.2.1 Phase blazing

It is advantageous to incorporate a blazed grating phase pattern to the required phase profiles while constructing phase modulation plates, to spatially split the modulated modes from unmodulated light during interaction with a phase modulator. This unmodulated part can happen due to direct reflection from the SLM display's surface. Both for DOEs and SLMs, the quantization of the phase can also be the reason for some unmodulated illumination.

When we did not add a blazed grating, the unmodulated beam can travel along the same direction as the modulated beam, spoiling the desired outcomes on the input light of a phase modulation pattern [67]. The use of blazed phase modulation patterns is essential in beam modelling implementations and here in this thesis we have used this with SLM for LG and Bessel beam generation. The phase in the blazed grating is varying from zero to maximum in a single period while in the binary grating (unblazed) the phase has only two values as depicted in figure 2.7.

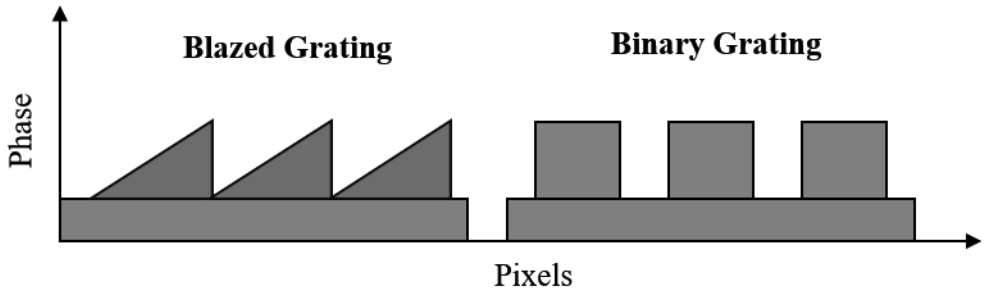

Figure 2.7: Schematic diagram of a blazed and unblazed (binary) grating.

Examples of blazing phase patterns are shown in figure 2.8 to transform the LG_0^0 mode to helical modes LG_1^0, LG_2^0 *and* LG_3^0. The angle of the blaze is decided such that the angle of diffraction in the 1st order is larger than that of the angle of divergence of the beam. Since, many phase patterns modulating tools have some spatial distinct level of mode separation, caution should be taken to prevent overlapping of higher orders with the 1st order of diffraction from the unblazed phase grating to ensure high quality in the required order of diffraction.

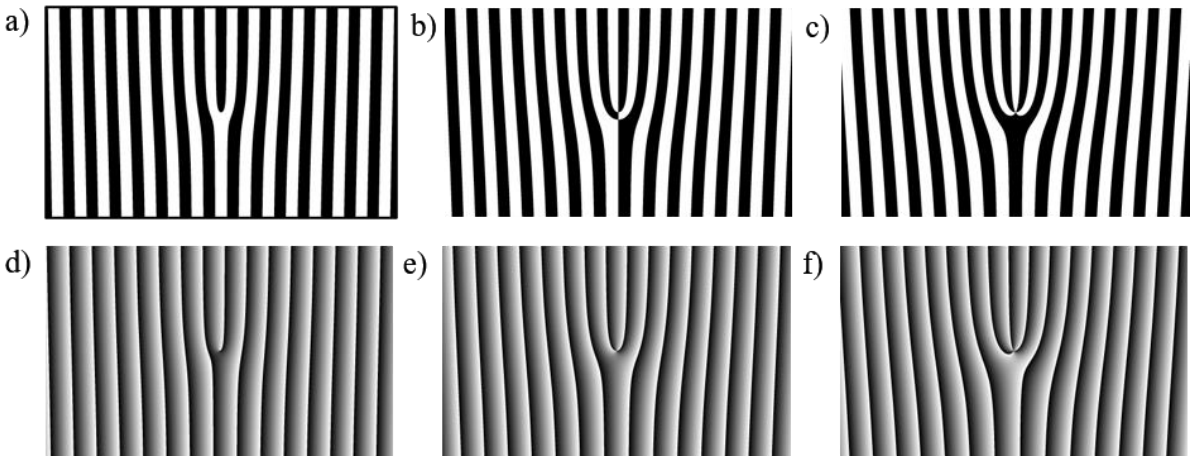

Figure 2.8: Forked diffraction grating: binary (a-c) and blazed (d-f) grating for l = 1, l = 2 and l= 3.

2.3 Generation of hologram for LG beam

Here we have simulated the forked diffraction gratings for LG beam generation using the above discussed theoretical approach for hologram generation. In figure 2.9 (a-c), the first column shows the linear phase ramp, the second column shows the spiral phase and the combination of the first and second columns which gives the 'forked' holograms to generate optical vortices for 'p' = 0 and l = 1, l = 2, and l = 3.

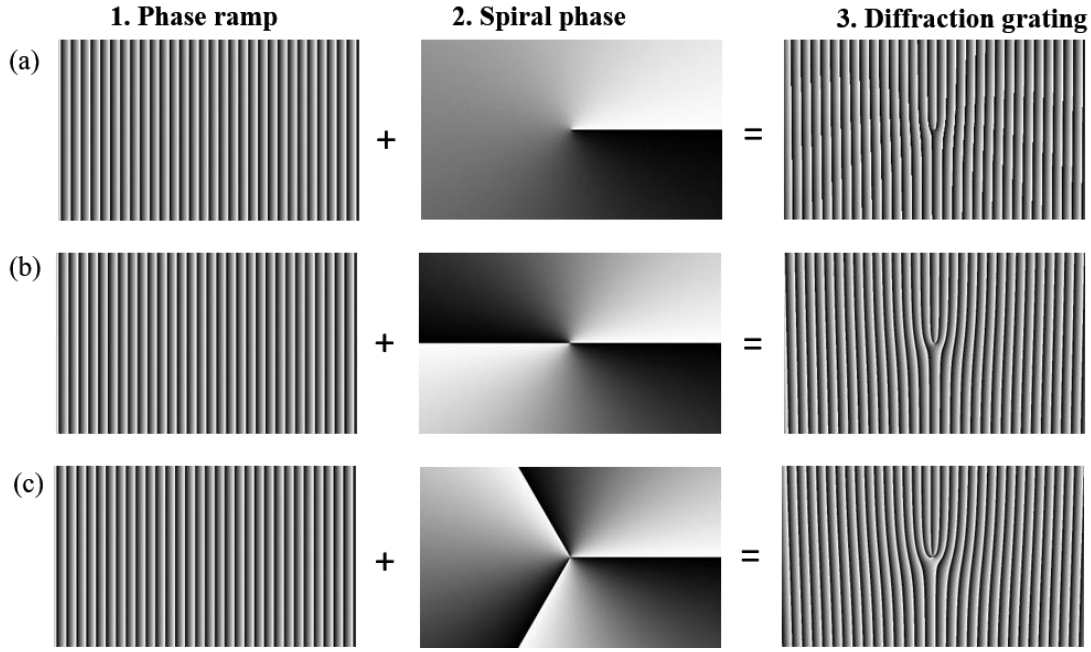

Figure 2.9: Simulated (1) phase ramp, (2) spiral phase plate and (3) corresponding forked diffraction grating for LG beam of l = 1 (a), l = 2 (b) and l = 3 (c). Phase levels are represented as grey value.

The similar approach is used to simulate the forked diffraction grating for higher-order radial modes of LG beams (LG_1^2, LG_1^3) as shown in figure 2.10. In higher-order radial LG modes, the index 'p' is introduced which is used to generate nodes in the radial direction. Figure 2.10 (a) is for LG_1^2, which has index p = 2, used to create two radial nodes and figure 2.10 (b) is for LG_1^3, which has index p = 3, used to create three radial nodes.

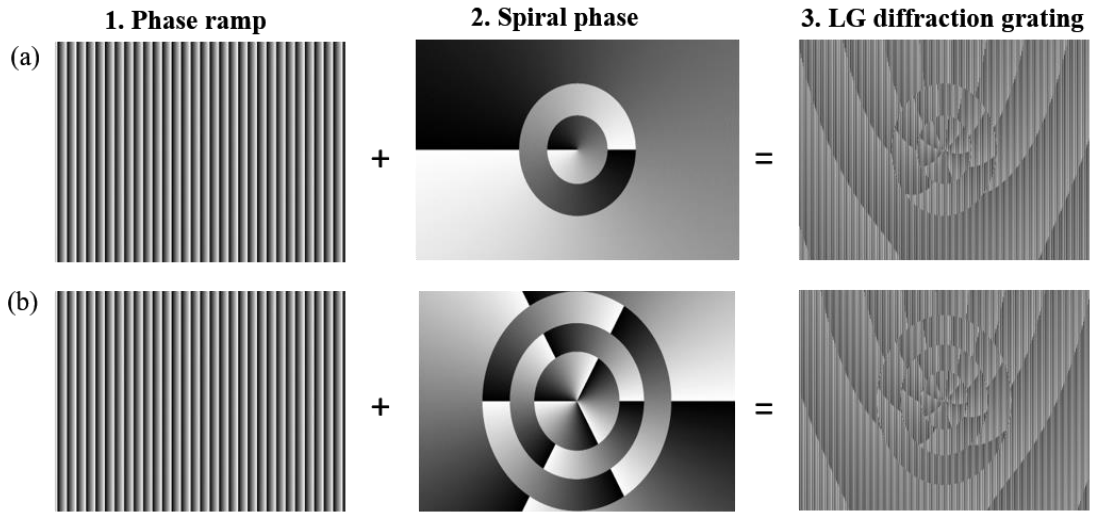

Figure 2.10: Simulated diffraction grating (1), phase plate (2) and corresponding forked diffraction grating (3) for higher-order radial LG modes, (a) LG_1^2, (b) LG_1^3.

2.4 Generation of hologram for Bessel beams

As shown in figure 2.11 (a) diffraction grating for the Bessel beam is simulated in similar fashion by adding an axicon phase to the forked grating. For zeroth order mode, since it has no singularity at the center as we have discussed, axicon phase is added to the diffraction grating. For higher-order modes of Bessel grating is replaced by a forked diffraction grating which will generate a singularity at the center.

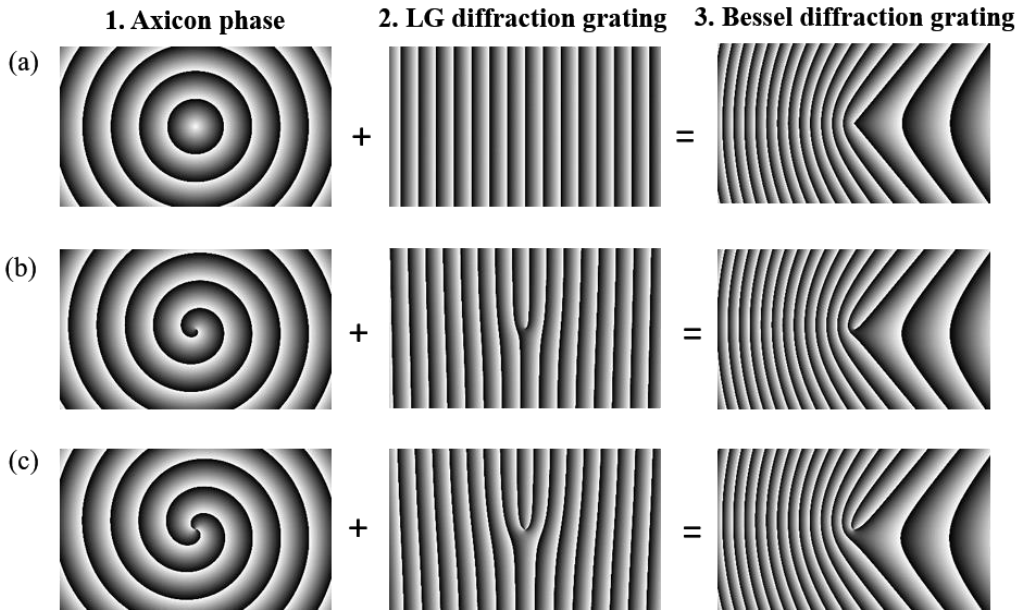

Figure 2.11: Simulated gratings for Bessel beam generation of different orders (a) J_0, (b) J_1, and (c) J_2.

2.5 Three-Dimensional visualization of LG beam using COMSOL

In the area of wave optics, large optical systems in a manner that rigorously resolves Maxwell's equation are challenging to simulate. This is because the waves that appear in the system need to be resolved by a sufficiently fine mesh. One alternative to this end is the use of a beam envelope approach in the COMSOL Multiphysics software. Apart from the experimental analysis of these beams, in this section of the thesis, we discuss how to use and control the electromagnetic waves system, beam envelopes in COMSOL. Here, we have used COMSOL multiphysics software for three-dimensional visualization of intensity, phase, and propagation properties of the OAM beams particularly LG beam.

Sometimes it is difficult to simulate models that are large compared to the wavelength. There are various methods to handle large models for fixed wave optics problems. These techniques include the so-called diffraction formula for the beam propagation process, for example, the Fraunhofer equation, Fresnel Kirchhoff, and the diffraction formula Rayleigh-Sommerfeld, as well as the beam propagation process and the angular spectrum technique. The COMSOL Multiphysics software with beam Envelopes gives an effective solution of the Helmholtz equation in a context in contrast to these approaches. It can handle large models and significantly relax the need for meshing [68].

2.5.1 Simulations for LG beam

In this section, we have explained how COMSOL Multiphysics software can be used for the study of an OAM light. By reproducing the OAM beams in COMSOL via simulation, here we have supported our test results. COMSOL Multiphysics has therefore proved to be a very efficient means of visualization. It has allowed us to achieve accurate results in good agreement with the experiments.

The intensity and phase profiles of OAM beams with index l = -1, 0, 1, displayed in the x-y plane, are instead reported in figure 2.12. Such examples confirm the well-known features of OAM beams with index $l \neq 0$, characterized by an azimuthal phase variation of $2\pi |l|$ around the central axis of zero intensity, with a handedness dictated by the sign of l.

2.5.1.1 Intensity and phase profiles for LG modes

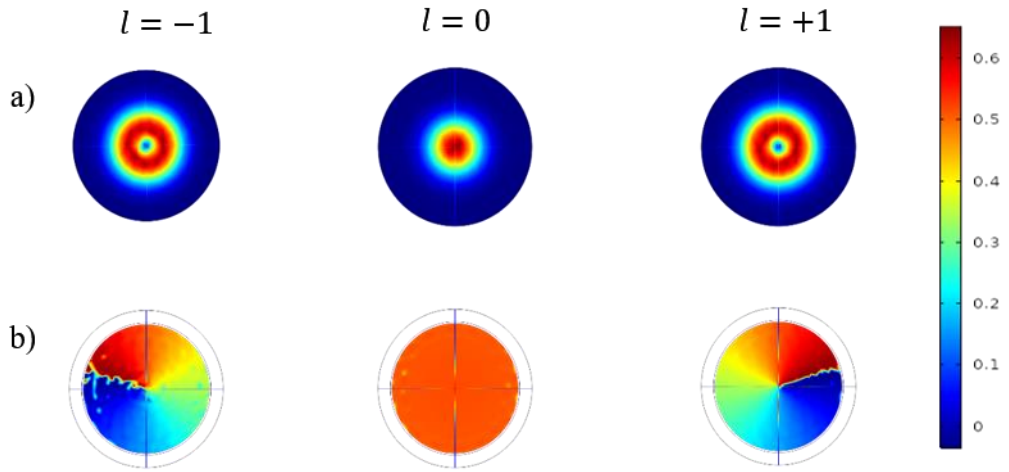

Figure 2.12: Intensity (a) and phase profiles (b) of the OAM modes with index l = -1, 0, 1 simulated using COMSOL.

The above figure 2.12 shows the intensity and phase profile for varying topological charge, l = 0 (which corresponds to a Gaussian beam), $l = -1$, and $l = +1$. Clearly for l = 0 the phase remains constant. However, we observed that the phase varies for the other two cases and in the opposite direction to each other. The evaluated electric field intensity propagation for LG_1^0 mode is shown in figure 2.13.

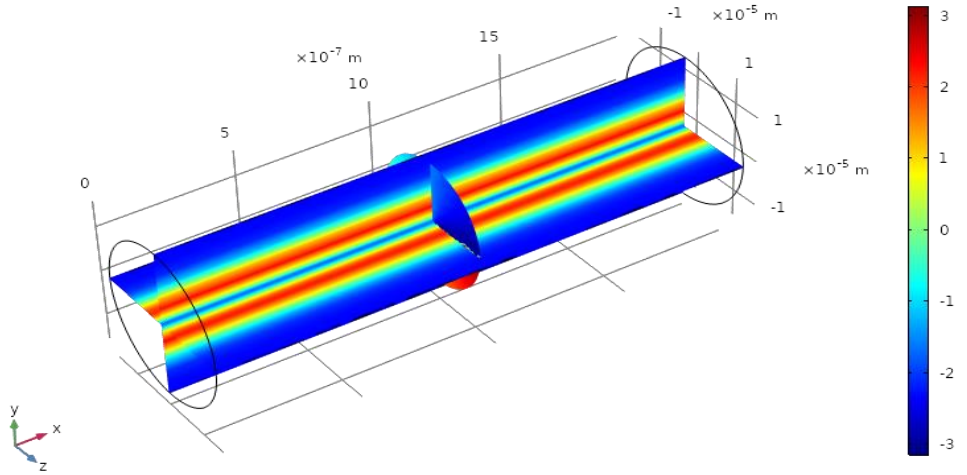

Figure 2.13: The electric field norm showing the ring structure of the beam for LG_1^0.

2.5.1.2 Visualisation of phase propagation

As discussed earlier, a vortex beam, typically represented by the Laguerre-Gaussian beam has a rotating phase around the optical axis as the beam propagates. This phase distribution produces a Gaussian donut beam as shown in figure 2.13.

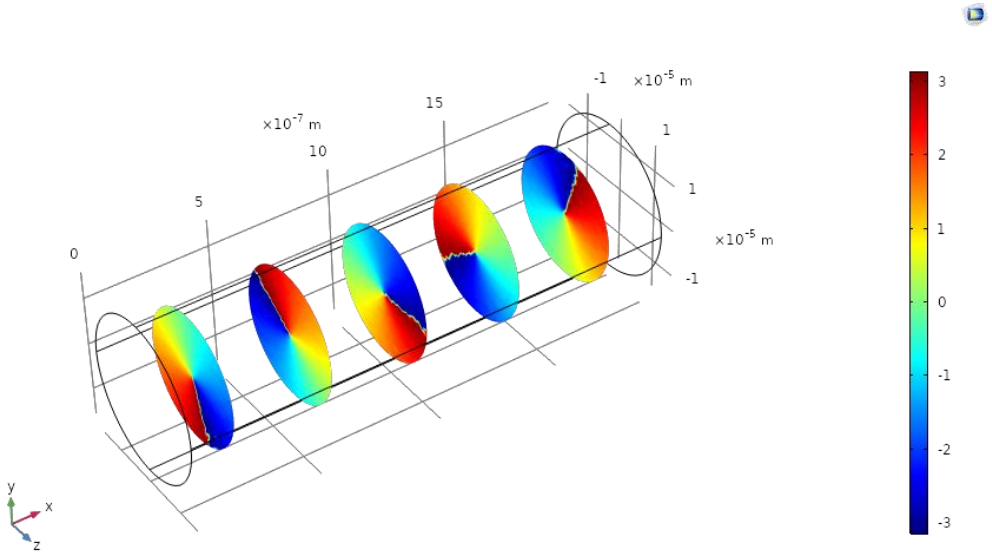

Figure 2.14: Phase distribution at five different locations along the direction of propagation for LG_1^0.

2.5.1.3 Visualisation of spiral phase variation of LG beam

As it has been discussed that the phase rotates around the optical axis as the beam propagates. The resulting beam also called a vortex beam or a helical beam has a spiral phase distribution. Figure 2.15 shows the 3D visualization of spiral variation of the phase for LG_1^0mode.

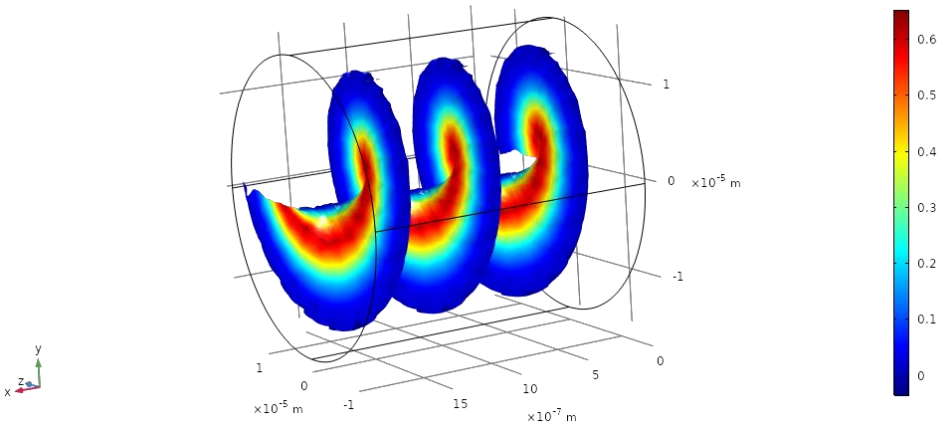

Figure 2.15: The spiral phase variation of the vortex (OAM) beam for LG_1^0mode.

Another way to generate a beam with OAM is by a spiral phase plate to give a Gaussian beam. Thereby, the beam which is transmitted will possess a helical wave-front, leading to a vortex beam. Also use of an SLM is one of the efficient methods (briefly discussed in this thesis).

2.5.1.4 Intensity and phase profiles for higher-order radial LG modes

Different modes of the LG beam are compared with each other to see how they are different from each other. Experimental results can only show us some visible features of these beams. However, theoretical model simulations for the same using software like COMSOL can help to visualize some complex features like phase, propagation in space for these beams. Here in figure 2.16, we have shown three modes of LG beam LG_1^0, LG_2^0, LG_3^0 simulated using COMSOL. The first row shows the intensity profile of these mode. As the topological charge increases, the dark region at the center (singularity) increases which we have further verified in the experimental section as well (see chapter 3). These modes have a variable phase from 0 to 2π at every cross-section of the propagating beam. Middle panel shows the variation of phase for different modes of LG, where for LG_1^0 the phase is rotating ones from 0 to 2π, whereas for LG_2^0 and LG_3^0 , it is rotating twice and thrice respectively around the singularity and the third row shows the 3D visualization for the same i.e. the spiral phase of the respective modes.

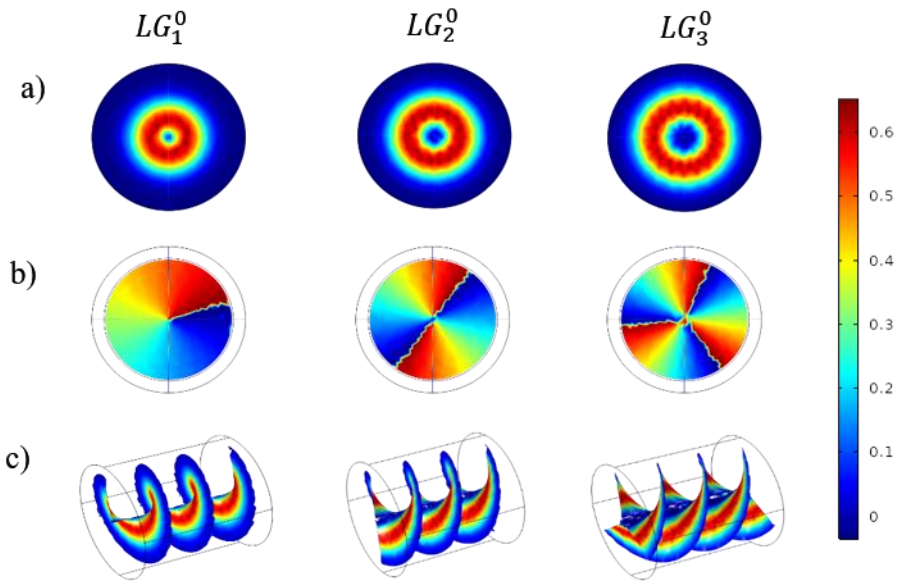

Figure 2.16: Intensities and phases for different modes of LG beam.

Chapter 3

Experimental Studies

3.1 Experimental set up:

Figure 3.1 shows the experimental set up which is used to generate LG and Bessel modes using SLM. Here, we have used a diode laser having a Gaussian beam profile after mode clean-up with a central wavelength around 655 nm. To clean the spatial mode we use mode clean up setup (combination of lens and a pinhole) and passes through a beam expander to fill the active region of the SLM (Model: 1920×1152 Analog SLM).. The SLM that we have utilized, was bought from Meadowlark Optics, having an active area cross-section of 1920×1152 pixels, with pixel size 9.2 μm × 9.2 μm. The SLM is then implemented with a desired CGH (discussed in Chapter 2) on to its screen to get the required LG and Bessel modes. The hologram on SLM generates a diffraction pattern and the desired mode is at the first order of the diffraction which is recognized with an image sensor (we have used a beam profiler camera from Newport, Model: LBP2-VIS2) to analyse the beam profiles.

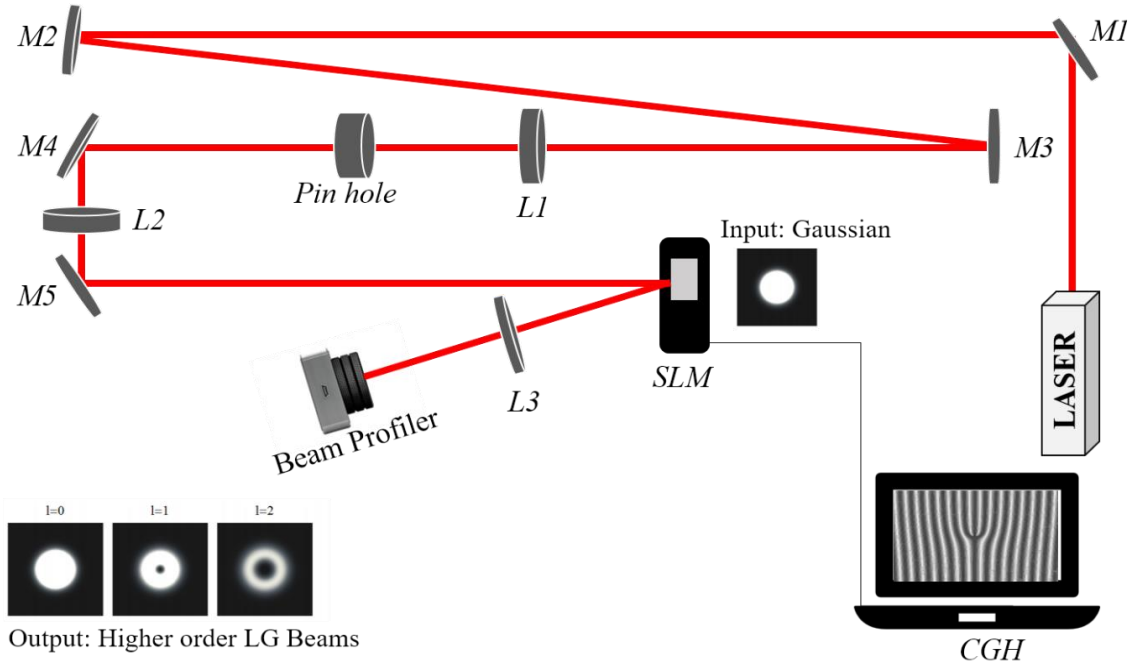

Figure 3.1: Schematic of the setup used for the generation of the LG beam generation using an LCOS-SLM.

Figure 3.2 shows the picture of the setup, we have in our lab. Where we have demonstrated the beam path originating from the source (diode laser) and passing through various optics and reaching to the SLM screen. After reflection from the SLM screen, the different modes of the modulated output beam are recorded, analysed and confirmed. All these are discussed in detail in the following sections of this chapter.

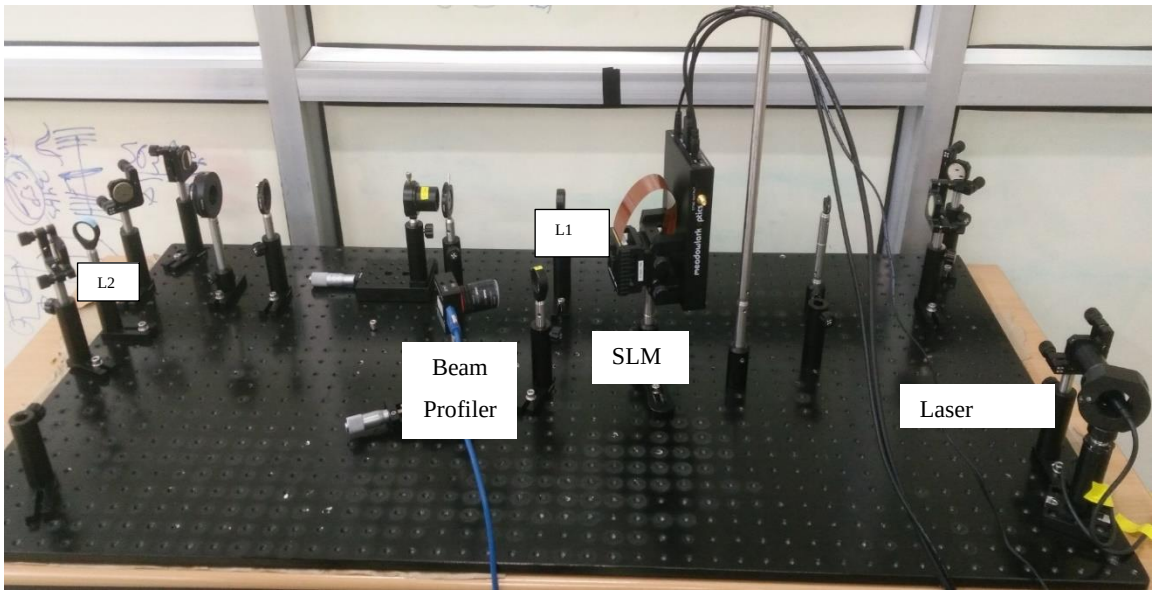

Figure 3.2: Table top showing the optical path of the laser beam.

3.1.1 Mode clean up

There are several reasons due to which a laser beam often has an imperfect beam quality, which means there are many distortions in the intensity/phase profile of the beam. Various kinds of "mode cleaner" methods are often used for "cleaning up" the beam profile depending upon the requirement. These mode cleaners are usually of two types resonant and non-resonant. Both of them have their respective operational principles and applications.

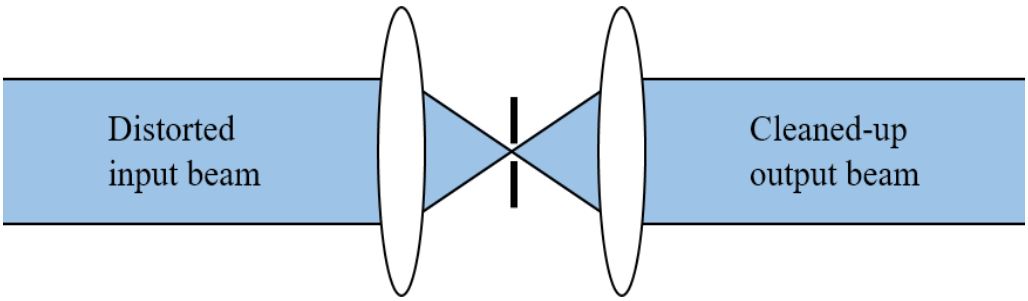

Figure 3.3: Mode cleaner set up having two lenses and a pinhole.

Figure 3.3 shows the schematic of the non-resonant mode cleaner set up using a pinhole and a combination of two lenses which we have used in our experiments. From the left-hand side, the distorted beam is coming and falling on the first lens, which is then made to focus on a small spot, passes through a pin hole, and again collimated through the second lens. To get the maximum power after mode clean-up, we have used the different

combinations of lenses and the size of pinholes. The figure 3.4 (b) shows the beam profile after mode clean-up and expanded.

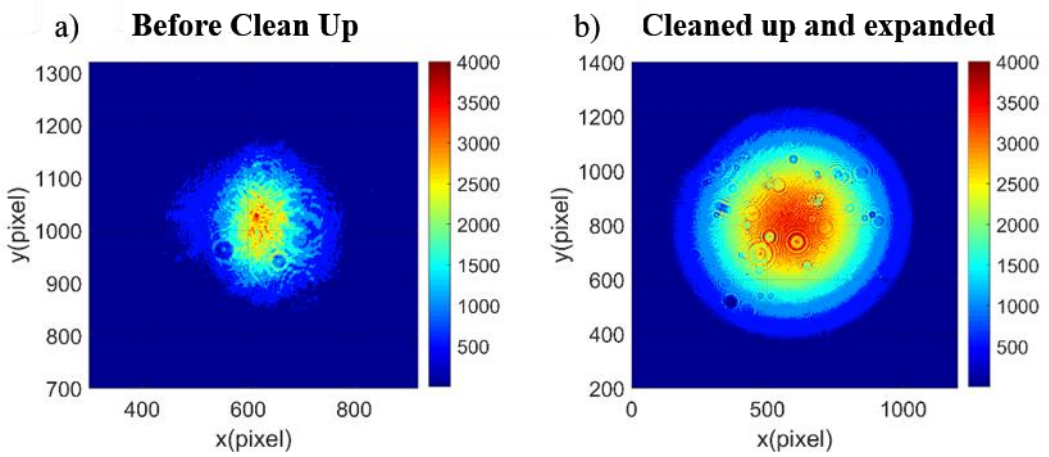

Figure 3.4: Intensity profile for laser output before and after mode clean up.

3.2 Experimental results

3.2.1 Generation of LG modes

We have illustrated here the holographic generation of higher-order LG beams which are generated using the SLM. As discussed in Chapter 2, the details of the hologram pattern generation, to ensure that these holograms work as expected, we employed the simulated forked grating on the SLM screen and analysed the pattern of the output beam. We have confirmed the generation of the LG modes using interferometry which is discussed later in this chapter. In addition, we have simulated the intensity profiles of the output modes for the better understanding the LG modes, which can be seen in figure 3.5 (a-c). We have simulated intensity profiles of LG modes for different 'l' indices i.e. azimuthal order and compared with those experimentally obtained as shown in figure 3.5 (d-f). In this section, we have shown the results which were obtained using input as a Gaussian beam profile. Figure 3.6 shows the LG beam patterns, which are multi-ringed intensity profiles for different 'l' and 'p' values azimuthal and radial indices respectively. The symmetrically even shapes of the resulting beam patterns prove that the aberration of the optical system is sufficiently removed to study the output beam quality. In this manner, we have got a nice agreement between the theoretical and experimental results by illuminating the CGHs with Gaussian profiles.

3.2.1.1 Intensity profiles of zero-radial order OAM modes

Figure 3.5 shows the intensity distribution in the x-y plane for different azimuthal order, (a) l = 1, (b) l = 2, and (c) l = 3, keeping radial order p = 0. It can be evident that l = 0 gives pure Gaussian, as discussed in chapter 2. A beam with l = 1 resembles a doughnut with a node/singularity at the center of the beam. Here, we can see that the central region or waist size keeps on increasing with an increase in the value of 'l'.

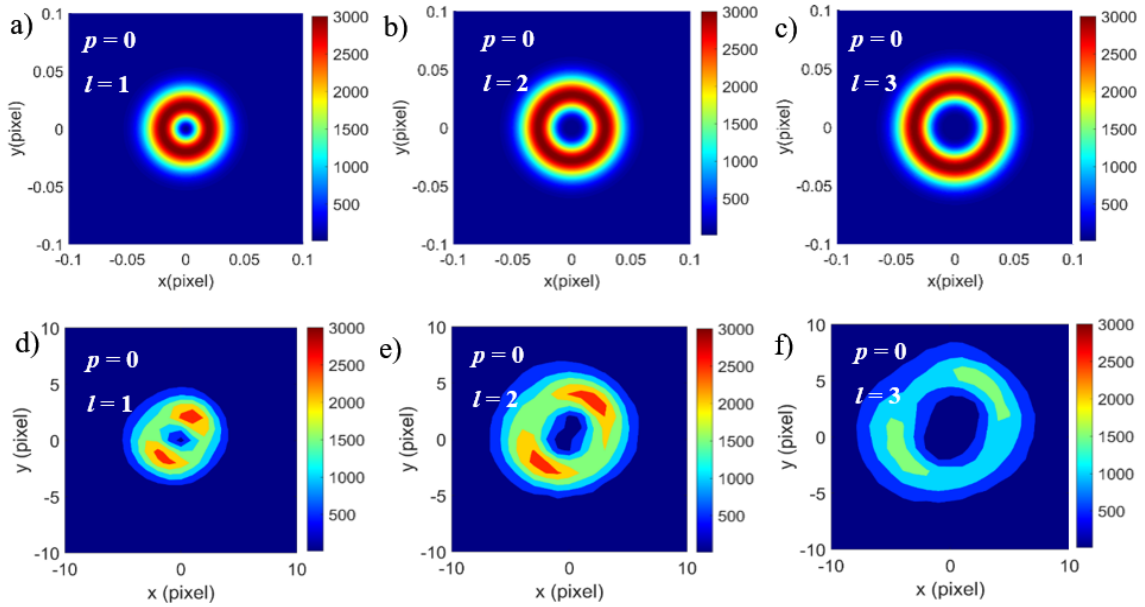

Figure 3.5: Theoretically simulated (a-c) and corresponding experimentally generated (d-f) helical LG modes patterns generated from the Gaussian input beam.

3.2.1.2 Intensity profiles of Higher-radial order LG modes

Figure 3.6 shows the field distribution in the x-y plane for (a) $p = 2$, (b) $p = 3$, corresponding to first azimuthal order, i.e. l = 1. Here, we can see that the central region or waist size remains the same while keep on increasing the value of 'p'. However, the number of rings surrounding the central regions increases.

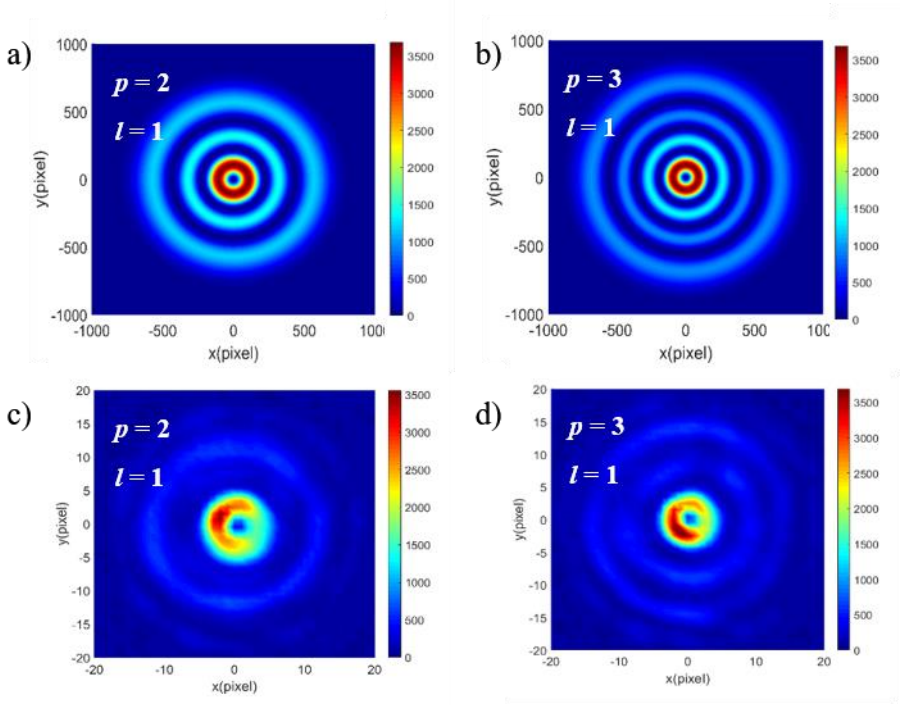

Figure 3.6: Theoretically simulated higher-order LG modes (a-c) and Intensity profiles of experimentally generated helical LG modes by the interaction of a LG_0^0, with the phase modulation profile (c-d) for $LG_1^2$and LG_1^3.

We can very well observe some asymmetry in the experimental intensity profiles. It might be due to aberration or the complex shift in the phase profile or the input beam may not have been in a pure Gaussian mode, but the reason for this is not entirely clear. We found that changing the alignment of the hologram on the SLM did not clear up this problem. Also, it is interesting to note that in figure 3.6, the first diffracted beams appear to be getting less intense as the order of LG increases from p = 2 to p = 3. The simplest explanation for this trend is illuminated by figure 3.5, where profiles of the first diffracted beams are shown on the same scale for varying azimuthal index l = 1, l = 2, and l = 3 hologram. Also, from figure 3.5, it's clear that as l increases, the waist size of the output beam increases. Assuming that the same amount of power is channelled into the first diffracted beam for each 'l' value, consequently, the same amount of power is being spread over larger areas for larger 'l' value. Here, the output beam seems less intense for larger 'l'. So, to get an exact agreement among the experimental and the theoretical simulated results, there are several other factors governing it and it is difficult to pinpoint one of the impacts.

3.2.1.3 Intensity distribution of LG modes

Apart from plotting the observed mode pattern, we have also plotted the cross-sectional profiles of both zero-order radial OAM modes, as shown in figure 3.7 (a-c) and higher radial order of LG modes, as shown in figure 3.7 (d-e).

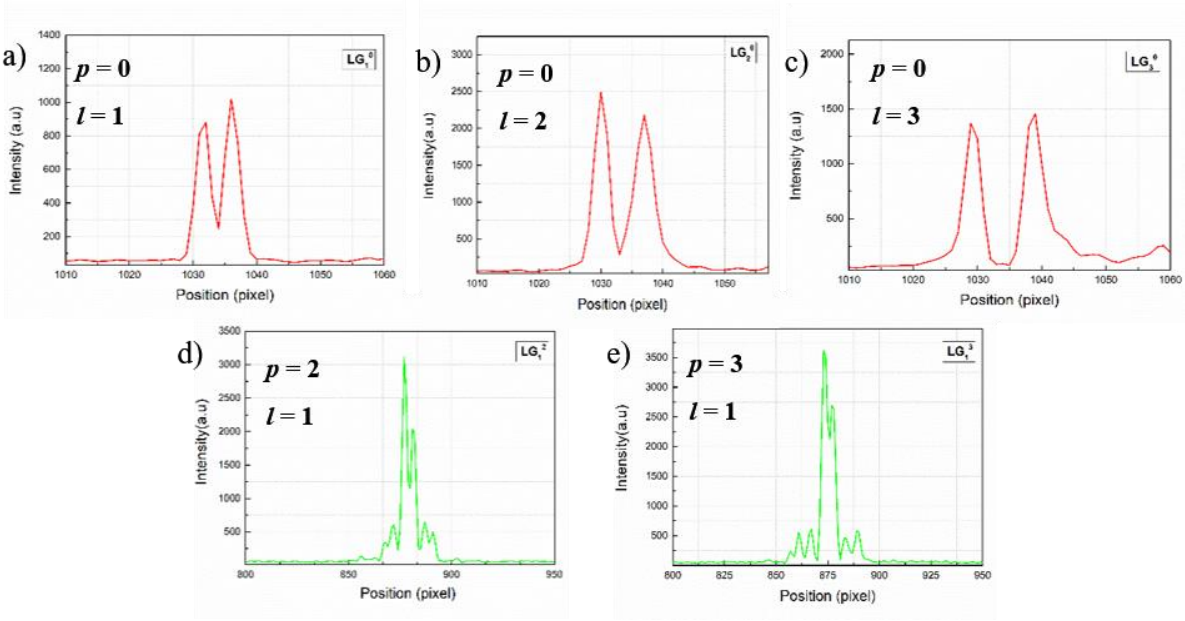

Figure 3.7: Cross-sections of the intensity distribution of observed mode patterns for higher-order radial LG modes over pixel position (a) LG_1^0, (b) LG_2^0, (c) LG_3^0, (d) $LG_1^2$and (e) LG_1^3.

3.2.1.4 Effect of fringe density on the intensity of generated LG modes

Fringe density is one of the important parameters of Hologram generation. Fringe density is basically, line density and is represented by symbol ‘s’. Also, mathematically we can define the fringe density with the help of following relation, where it varies with the number of pixels per unit line on the SLM screen.

$$\frac{1}{s} = \frac{Pixel}{line} \tag{3.1}$$

We have studied the effect of fringe density for LG_1^0mode, for which we generated different holograms having different fringe density value and we got the good intensity in the first order of diffraction which is generated LG beam for some of the ‘s’ value of hologram. Figure 3.8 shows the 3D intensity profiles for some of the ‘s’ values, and it can be observed that as the ‘s’ value increases, the intensity in the first order and the spacing between first and zero order of diffraction increases. We took the data for various ‘s’ values and noted that for s = 3.1(approximately multiple of π), we were able to record better mode intensities, which shows that the fringe density plays a crucial role in diffraction from the grating. However, no regular trend was observed with the variation of the fringe density.

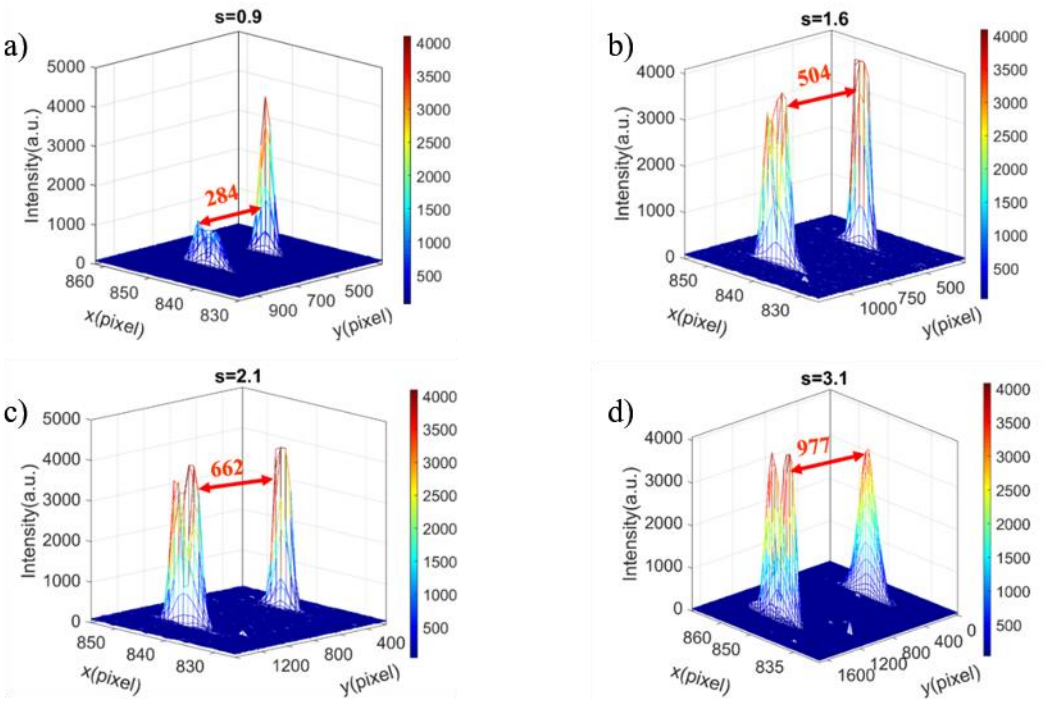

Figure 3.8: Intensity variation of a LG_1^0mode with varying 's' value.

3.2.1.5 Effect of phase blazing on the intensity of generated LG modes

We have additionally shown that it is helpful to include a blazed grating phase pattern to the initially required phase profile, to spatially isolate the modulated light from the unmodulated light during the interaction with the phase modulating device. Figure 3.9 shows two 3D intensity plots for a LG mode, obtained by using an unblazed and blazed hologram and we have observed better intensity in the latter case.

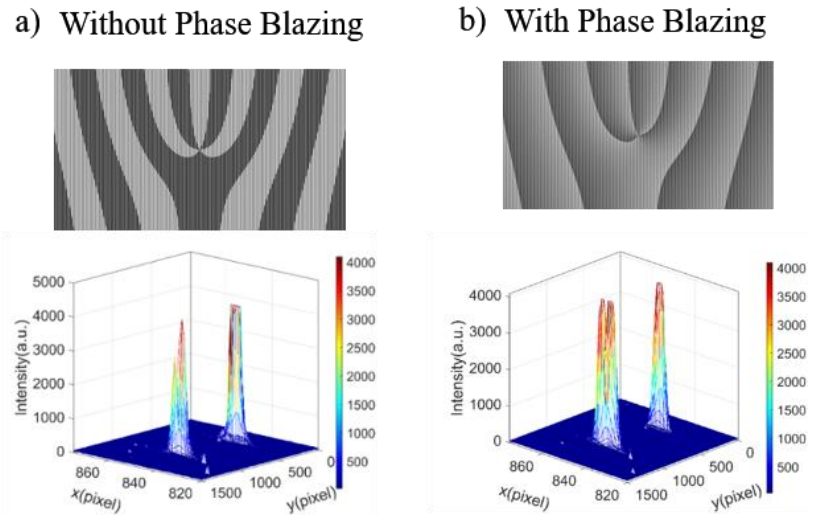

Figure 3.9: Effect of phase blazing on the intensity of generated LG modes.

3.2.1.6 Propagation of the LG beam

LG beams are well known to exhibit some unusual features, which make them suitable for a wide range of applications. In the last few decades, the focusing property of the LG beams become an important parameter and have recently gained a lot of attention and their uses have been reported in the diversity of fields ranging from material processing, microscopy, confinement of particles in optical traps, and for micro-manipulation applications because of their ability to transfer their OAM to particles. We studied the propagation of first order of LG beam and observed the variation of intensity profile and the rotation of intense lobes as shown in figure 3.10.

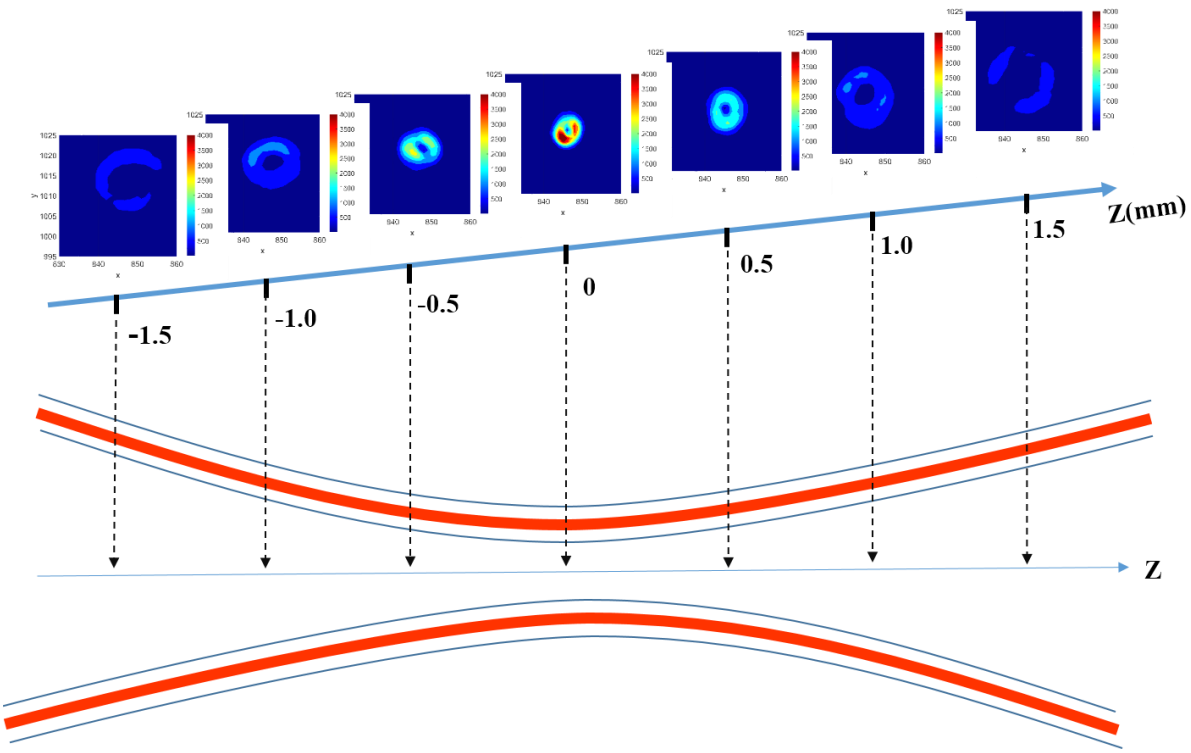

Figure 3.10: Tight focusing behaviour of a right-circularly polarized vortex LG beam with $l = 1$ in the vicinity of the focus.

Clearly, the propagation of an LG beam ($l = 1$) in space shows the change in the intensity of the beam along the Z-direction, which is found to be maxima at its focus.

3.2.2 Generation of Bessel modes

Here, we have shown the experimental results for the generated Bessel modes, by implementing the corresponding phase mask (discussed in chapter 2) on the SLM. For the generation of Bessel beams, we have utilized a linear phase modulation with axial symmetry, like an 'axicon'. Figure 3.11 (a-d) shows intensity profiles in camera plane (XY

plane) for zeroth, first, second, and third order Bessel beams respectively. Figure 3.11 (e-h) shows the cross-section of the intensity distribution for beam different orders of Bessel beam. Higher order Bessel beams generally have a phase singularity on the beam axis and hence exhibit a non-diffracting dark, rather than bright core.

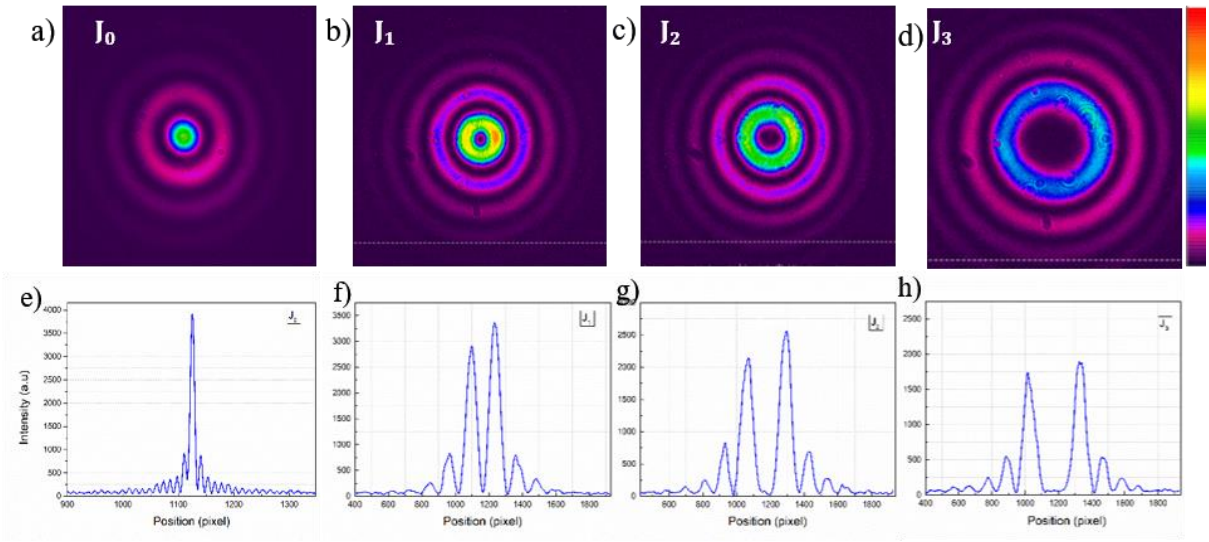

Figure 3.11: Intensity profiles of experimentally generated Bessel (a-d) and Cross-sections of the intensity distribution (e-h) for of observed mode patterns of different order (J_n) of the Bessel beam.

3.2.2.1 Free-space propagation of Bessel beam

Bessel beams are ideally considered as nondiffracting but in lab condition, there is a limit to it [62]. We have demonstrated the propagation of the zeroth order of the generated Bessel beam. We took the beam profile images at varying distances from the SLM, starting from 1.2 m to 3.5 m, to look into the non-diffractive nature of the beam. The results for the same are shown in figure 3.12. Here we can see that generated mode travel some distance without getting diffracted, almost up to 2.5 meters as it is clear from figure 3.12 (d) but after that, it reaches a limit and then rings keep on diminishing on increasing the distance, also at far-field we have observed an annular ring, which we have discussed later in detail in section 3.3.1 of this thesis.

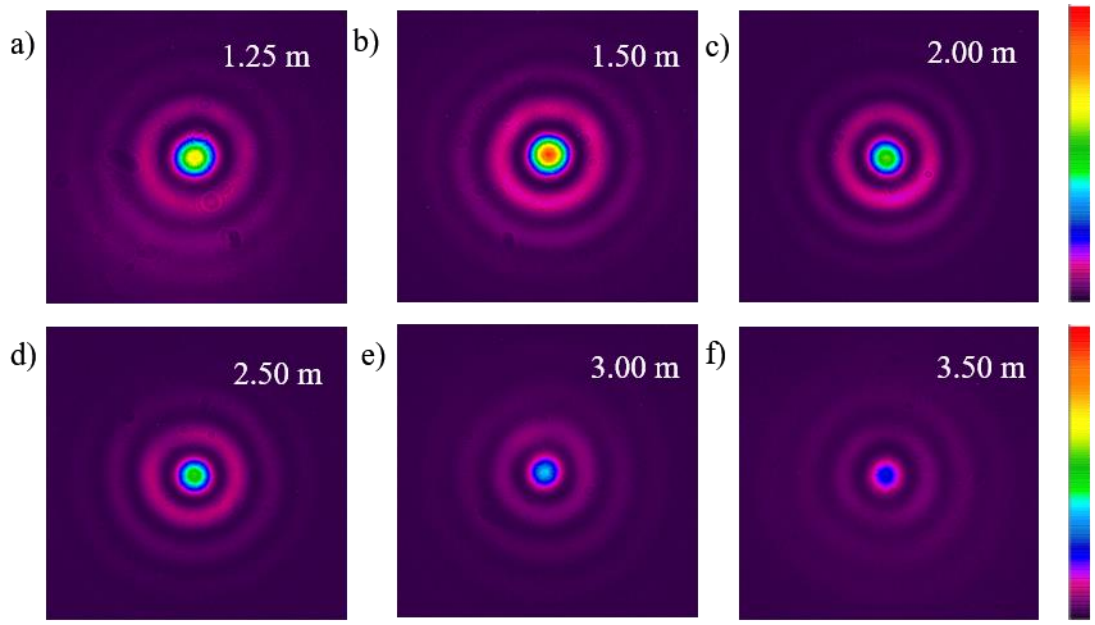

Figure 3.12: Free space propagation of the Bessel beam in space at distance (a) 1.25 m, (b) 1.50 m, (c) 2.00 m, (d) 2.50 m, (e) 3.00 m, and (f) 3.50 m.

3.3 Verification of generated modes

So far, we have obtained the LG and Bessel modes with Gaussian input with the help of a versatile beam shaping technique that employs theoretical hologram generation and implementation on to the SLM depending upon the desired output. After that, we have also worked towards verifying these output beams that we have obtained after implementing CGH with the Gaussian beam profile. For that, we have used different methods for both LG and Bessel mode verification which is discussed one by one.

3.3.1 Verification for LG modes

We have confirmed the phase profiles of the output beams by looking at the interference patterns of generated LG beams with the plane/spherical reference beam.

3.3.1.1 Interference with plane wave

Figure 3.13 shows the schematic outline utilized for the affirmation of LG modes by the interference of the acquired modes with the Gaussian fundamental beam as a reference beam in the plane waveform. Here, we have done few adjustments in the arrangement that we have priory examined for the generation of these beams, the only difference is that we kept a beam splitter (BS) in the way of the first Gaussian beam which split this Gaussian beam into two parts, out of which one is sent to the SLM to create the diffracted LG modes,

a mirror M6 is kept in the way of the other beam coming from the BS, and after reflection from the mirror M6, it arrives at the beam profiler camera. Additionally, 1st LG mode which is diffracted from the SLM is then likewise sent to the beam profiler alongside the Gaussian mode, to record their interference pattern.

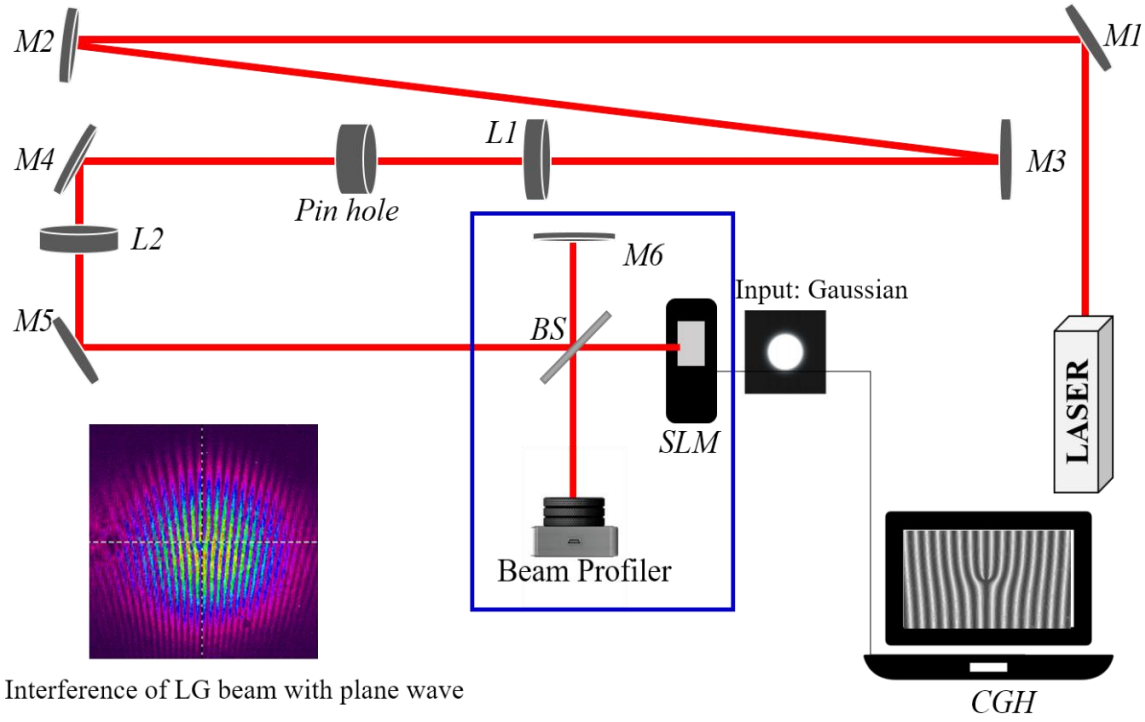

Figure 3.13: Schematic diagram of setup for interferometry using plane Gaussian beam.

The intensity distribution we have obtained after the interference of the two beams (Plane Gaussian and different LG modes) are in acceptable concurrence with that we anticipated, yet an inquiry stays concerning the phase structure of the beams created. Here, we have confirmed the phase profile of different LG modes that we earlier obtained with the SLM by looking at the interferograms resulting from the interference of the LG mode with the reference plane wave. Figure 3.14 shows the experimentally observed patterns that demonstrate clearly the phase profiles for the LG beams with SLM. Additionally, results we have obtained also shows a feature, which tells, that the obtained interferograms look like the forked grating and subsequent hologram we have implemented onto the SLM for their generation. The non-diffracted beam having the zeroth-order displays a plane-wave phase profile. However, the first-order beam in principal showed a solitary (single) fork at the edges, demonstrating $e^{i\varphi}$ type of phase profile. For the second-order beam, we have obtained an interferogram which exhibited a twofold fork, showing an $e^{i2\varphi}$ type of phase

profile. Similarly, the third-order mode displayed three branches in the fork demonstrating $e^{i3\varphi}$ phase [69].

So, the observed forked liked branches in the interference pattern between various LG modes reflected from the SLM screen and a LG_0^0 mode, as shown in figure 3.14, demonstrates a decent agreement to the phase profile used to create the LG modes. It is clear from the figure, the number of teeth in the fork corresponds to the 'l' value of the mode being reported.

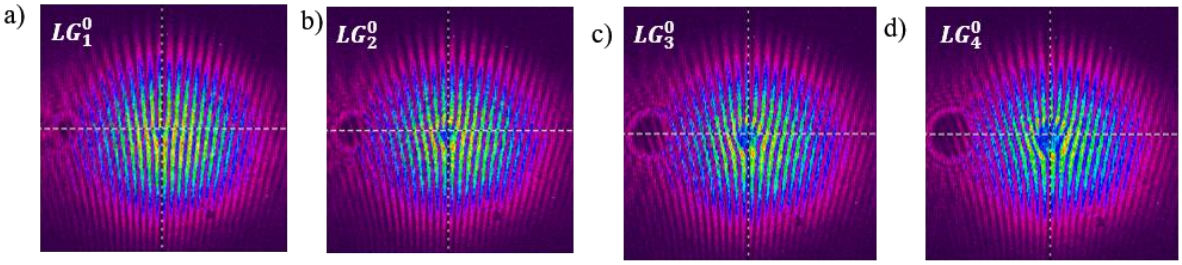

Figure 3.14: Experimental interferograms recorded for plane reference wave with different LG modes (a) LG_1^0, (b) LG_2^0, (c) LG_3^0, and (d) LG_4^0.

3.3.1.2 Interference with a spherical wave

Figure 3.15 outlines the schematic utilized for the affirmation of LG modes by the interference of the acquired LG modes with Gaussian beam as reference beam in spherical

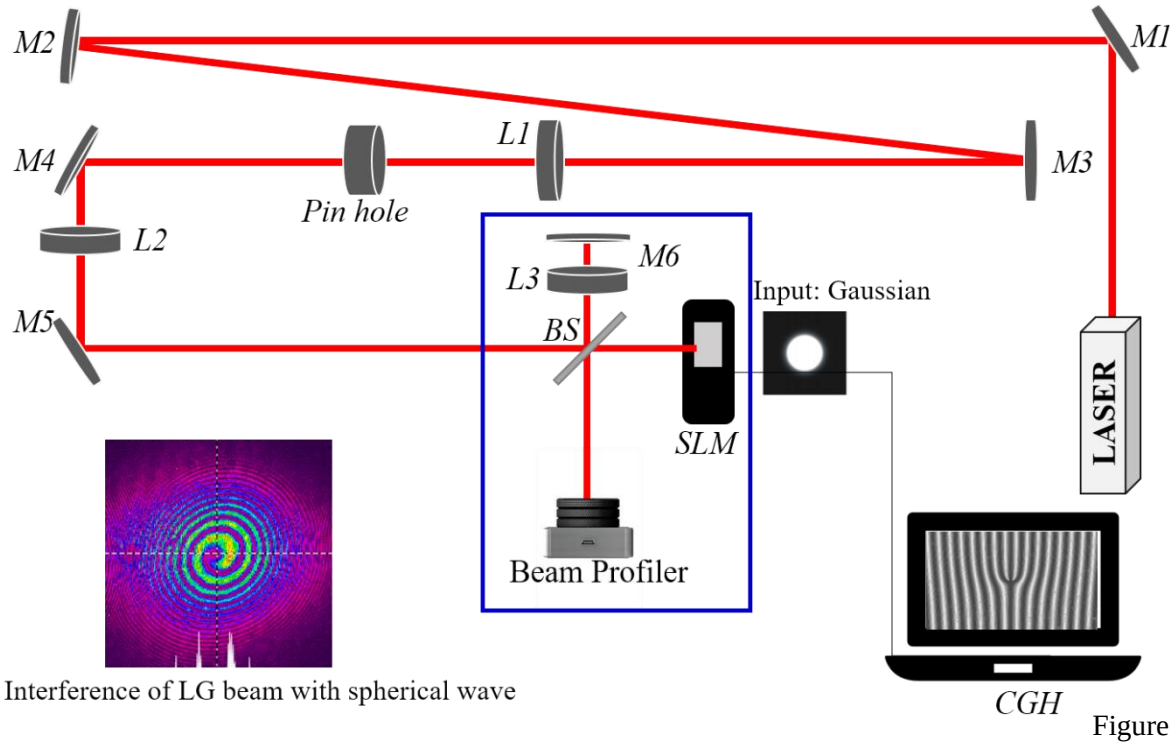

Figure 3.15: Schematic diagram of setup for interferometry using a spherical Gaussian beam.

waveform. The arrangement utilized for this situation is nearly equivalent to examine in section 3.3.1.1 (for plane reference wave). In this case, we kept a lens (L6) in the way of the beam which was reflected from the mirror (M6), to make a spherical waveform of Gaussian beam. This reference beam along with the picked diffracted mode, acquired from the SLM are made to interfere, and their interference patterns were recorded.

The interference of the fundamental beam having a spherical Gaussian profile with the LG beam is known to change the phase into the intensity distribution. So, whenever we interfered with these two beams, the phase of the LG beam, which was in helical pattern gets finally converted into a vortex kind of field, which has 'l' number of spirals in the obtained interferogram. Figure 3.16 (e-h) shows the pattern obtained for the interference between Spherical waveform Gaussian and LG modes with azimuthal index l = 1, 2, 3 and 4, obtained from the SLM which was displayed as the helical phase profiles of different modes of LG which clearly shows the formation of spirals in the interferogram. All the figures foresee the arrangement of a vortex kind of field at the center and show 'l' number of high-intensity spots. Additionally, the shape of these winding arms continuously changes at the central waist as it propagates. Here, we have also tried to simulate these interference patterns of fundamental Gaussian beam with the different order of the LG beam as shown in figure 3.16 (a-d). The striking component of every result shown is the winding/spiral behaviour observed in these interference patterns, displaying a few spiral arms whose number is equivalent to the azimuthal l order of the LG mode being reported. This spiral pattern is a normal result of the interference between the helical LG modes and the LG_0^0 mode with their respective phase fronts.

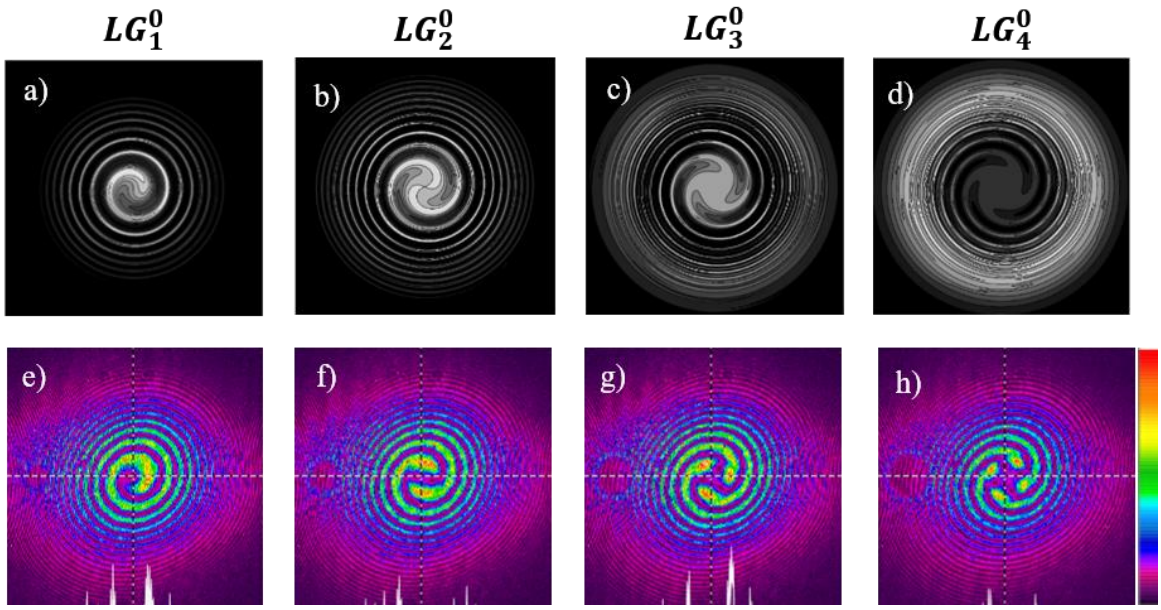

Figure 3.16: Results of simulated interferograms for 'spherical reference wave' with the ideal LG_l^p mode (a-d). Experimental results for the interference patterns recorded (e-h).

The interference patterns as displayed in figure 3.16 are found to be in good agreement with the recreated/simulated interferograms for almost all the LG modes, which demonstrates the correctness of the phase profiles obtained in the experiments.

3.3.2 Verification for Bessel modes

The property that has attracted the most attention of any non-diffracting or a Bessel beam is the results of the 'Bessel equation', which gives the following equality. It states that for the propagation of the Bessel beam in the z-direction, the intensity I, follows the given relation [58]:

$$I(x, y, z > 0) = I(x, y) \tag{3.2}$$

The above equality shows clearly that will be no change in the beam cross-section whenever it propagates and therefore, we concluded that the beam is diffraction free, or in other words, the propagation remains invariant. Another way of describing these is to consider them as a collection of several planar waves that are supposed to propagate on the surface of the cone as it is shown in figure 3.17 (c). Also, each of these propagating plane waves experiences an equal phase shift which is equal to $k_Z \Delta_Z$ and remains the same over a distance of Δ_Z. This kind of disintegration of these beams into many planar waves results

in the appearance of the annular ring kind of structure in the far-field, which is also be seen as a ring in k-space, as illustrated in figure 3.17 (b).

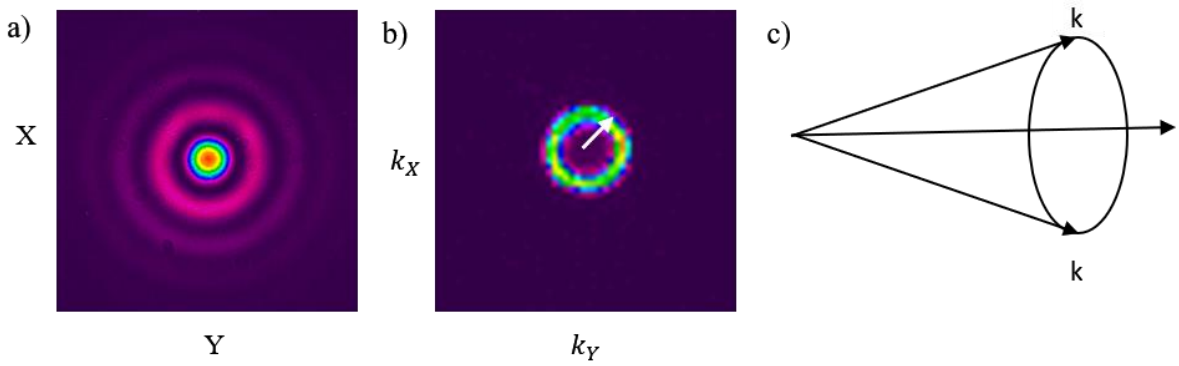

Figure 3.17: (a) Intensity profile for the Bessel beam, (b) Annular ring produced at the far-field (c) Propagation of the k-vectors on the surface of a cone.

So, for the confirmation of the generated Bessel beam, we have observed an annular ring in the propagation of beam at a distance of around 5 meters which might be the Fourier transform of the Bessel beam. We have performed the focusing of the generated Bessel beam and we got the annular ring at the focal plane similar to that obtained at the far-field, which is a well-known property of the Bessel beam as shown in figure 3.19 (a) and figure 3.19 (b) respectively.

Furthermore, we have demonstrated another method to justify the formation of the annular ring at the far-field upon Fourier transform of the beam in space, by doing the reverse of the above procedure.

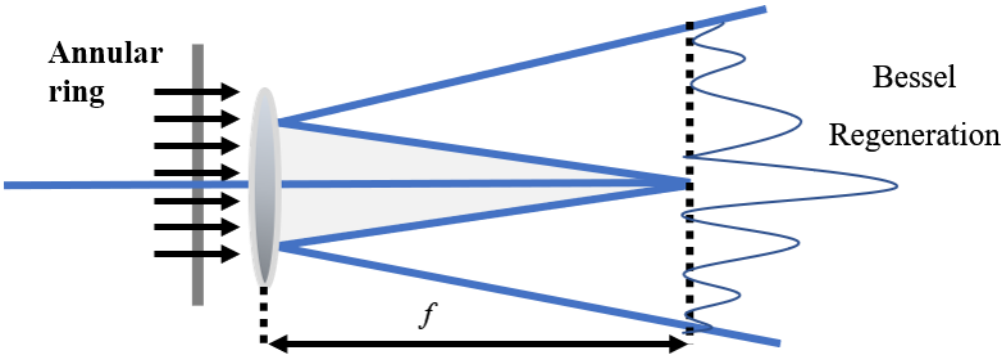

Figure 3.18: Schematic of set up to demonstrate the confirmation of output Bessel mode.

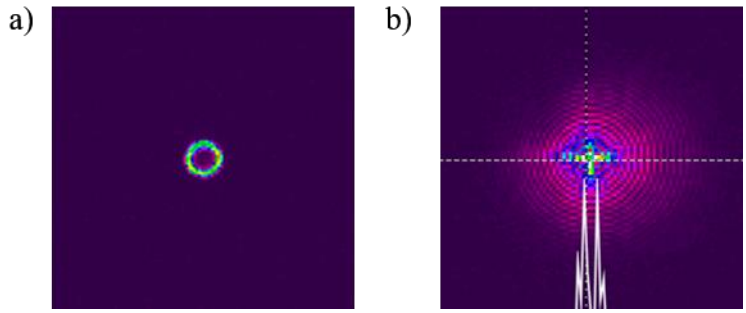

Figure 3.19: (a) Annular ring (At far-field) and (b) Intensity of beam produced at the backside focus of the lens.

The setup used for this purpose is shown in figure 3.18. Here, a lens is placed in the path of the annular ring that is formed at the far-field and observed the looked into the pattern of the obtained beam, which was recorded back-side focal plane of a converging lens, and then we looked into the pattern of the obtained beam. We have recorded the clear formation of Bessel modes, donated by Bessel regeneration in figure 3.19 has z_{max} distance of propagation, which verified that the modes that have been generated initially with the help of SLM were correct.

Chapter 4

Conclusion and future directions

4.1 Concluding remarks

Beam shaping is a very effective tool when it comes to the field of optics. The SLM along with the coupled program can be used to generate any type of hologram. Therefore, the SLMs could be pivotal for generating different modes of light. In summary, here we have demonstrated the generation of higher-order LG modes and Bessel modes from the Gaussian beam as input using reflective type LCOS-SLM implemented with computer-generated holograms. Since SLM comes with the advantage of producing desired phase modulation, mode patterns for various multi-ringed LG beams were universally reproduced. Moreover, we have also reported the confirmation of the generated LG and Bessel modes by theoretical as well as experimentally using a reference beam. The present approach provides a good beam shaping method for the generation of these modulated beams which can be employed for different applications such as optical manipulation, atom guides, optical traps, etc.

4.2 Future Directions

So far, we have presented a technique of beam shaping using SLM and successfully generated beams like LG and Bessel beam. Our next aim is to incorporate these beams into optical tweezer. Ultimately, SLM possesses a great advantage in optical tweezers setups because of its adaptability, as they hold a good potential of providing positional stability to the optical traps. Optical tweezers mostly use a standard Gaussian profile for the trapping of the particles. However, LG beams that possess OAM has emerged as a better candidate for use in optical tweezers [70]. There is plenty of work still to be done in this field and we have anticipated that our future work of incorporating these beams into the optical tweezer would help us investigate many problems like trapping of low-refractive-index particles with significantly enhanced trapping efficiency, trapping of particles that are optically reflective and absorptive, looking into rotational and twisting properties of particles which are challenging using Gaussian beam profile.

Bibliography

[1] History of Solar Energy, Solar Energy Technologies Program, Office of Energy Efficiency and Renewable Energy, U.S. Department of Energy, Washington, D.C., 2004. http://www.eere.energy.gov/solar/pdfs/solar_timeline.pdf.

[2] 2003 Annual Report of the International Energy Agency Solar Heating and Cooling Programme, Edited by Pamela Murphy, Morse Associates Inc., 1808 Corcoran Street, NW, Washington, DC, 20009 USA. A copy of this report is available online at http://www.iea-shc.org/.

[3] Claus, A.C. On Archimedes' Burning Glass; *Appl. Opt*. **1973,** 12.10, 14.

[4] Stavroudis, O.N. Comments On: On Archimedes' Burning Glass; *Appl. Opt*. **1973,** 12.10, 16.

[5] Cobble, M.H. Theoretical Concentration for Solar Furnaces; *Solar Energy* **1961**, 5.2, 61.

[6] Kamada, O. Theoretical Concentration and Attainable Temperature in Solar Furnaces; *Solar Energy* **1965**, 9.1, 39-47.

[7] Hassan, K.-E.; El-Refaie, M.F. Theoretical Performance of Cylindrical Parabolic Solar Concentrators; *Solar Energy* **1973**, 15, 219-244.

[8] Zakhidov, R.A.; Vainer, A.A. Distribution of Radiation Produced by a Paraboloidal Concentrator; *Appl. Solar Energy* **1974**, 10.3, 34-40.

[9] Jones Jr., R.F. Collection properties of generalized light concentrators; *J. Opt. Soc. Am.* **1977,** 107.11, 1594-1598.

[10] Winston, R. High Collection Nonimaging Optics; *Proc. SPIE* **1989,** 1038.

[11] Winston, R. Principles of Solar Concentrators of a Novel Design; *Solar Energy* **1974,** 16, 89-95.

[12] Winston, R.; Hinterberger, H. Principles of Cylindrical Concentrators for Solar Energy; *Solar Energy* **1975**, 17, 255-258.

[13] Burkhard, D.G.; Shealy, D.L. Design of Reflectors Which Will Distribute Sunlight in a Specified Manner; *Solar Energy* **1975**, 17.1, 221-227.

[14] McDermit, J.H. Curved reflective surfaces for obtaining prescribed irradiation distributions; Ph.D. Dissertation,University of Mississippi, **1972**.

[15] Horton, T.E.; McDermit, J.H. Optical Design of Solar Concentrators; *J. Energy* **1980,** 4.1, 4-9.

[16] Shealy, D.L.; Berg, H.M. Simulation of optical coupling from surface emitting LEDs; *Appl. Opt.* **1983**, 22.11, 1722-1730.

[17] Gabardi, D.R.; Shealy, D.L. Coupling of domed light-emitting diodes with a multimode step-index optical fiber; *Appl. Opt.* **1986,** 25.19, 3435-3442.

[18] McDermit, J.H.; Horton, T.E. Reflective optics for obtaining prescribed irradiative distributions from collimated sources *Appl. Opt.* **1974,** 13.6, 1444 –1450.

[19] Burkhard, D.G.; Shealy, D.L.; Sexl, R.U. Specular Reflection of Heat Radiation from an Arbitrary Reflector Surface to an Arbitrary Receiver Surface; *Int. J. Heat Mass Transfer* **1973**, 16, 271-280.

[20] Burkhard, D.G.; Shealy, D.L. View Function in Generalized Curvilinear Coordinates for Specular Reflection of Radiation from a Curved Surface; *Int. J. Heat Mass Transfer* **1973**, 16, 1492-1496.

[21] Schruben, J.S. Analysis of rotationally symmetric reflectors for illuminating systems; *J. Opt. Soc. Am.* **1974**, 64.1, 55-58.

[22] Burkhard, D.G.; Shealy, D.L. Specular aspheric surface to obtain a specified irradiance from discrete or continuour line source radiation: design; *Appl. Opt.* **1975,** 14.6, 1279-1284.

[23] Burkhard, D.G.; Shealy, D.L. A Different Approach to Lighting and Imaging: Formulas for Flux Density, Exact Lens and Mirror Equations, and Caustic Surfaces in Terms of the Differential Geometry of Surfaces; *Materials and Optics for Solar Energy Conversion and Advanced Lighting Technology*; *Proc. SPIE* **1986,** 692, 248-272.

[24] Gordon, J.M.; Rabl, A. Reflectors for uniform far-field irradiance: fundamental limits and example of an axisymmetric solution; *Appl. Opt.* **1998,** 37.1, 44-47.

[25] Westcott, B.S.; Norris, A.P. Reflector synthesis for generalized far-fields; *J. Phys. A: Math. Gen*. **1975**, 8.4, 521-532.

[26] Brickell, F.; Westcott, B.S. Reflector design for two-variable beam shaping in the hyperbolic case; *J. Phys. A: Math.Gen.* **1976,** 9.1, 113-128.

[27] McDermit, J. H.; Horton, T. E. Reflective optics for obtaining prescribed irradiative distributions from collimated sources; *Appl. Opt*. **1974**, 13, 1444-1450.

[28] Malyak, P. W. Two-mirror unobscured optical system for reshaping the irradiance distribution of a laser beam; *Appl. Opt.* **1992**, 31, 4377-4383.

[29] Shealy, D. L.; Chao, S. H. Design and analysis of an elliptical Gaussian laser beam shaping system; *Laser Beam Shaping II*; Dickey, F. M.; Holswade, S. C.; Shealy, D. L.; *Proc. SPIE* **2001,** 4443, 24-35.

[30] Frieden, B. R. Lossless conversion of a plane laser wave to a plane wave of uniform irradiance; *Appl. Opt*. **1965,** 4.11, 1400-1403.

[31] Kreuzer, J. L. Coherent light optical system yielding an output beam of desired intensity distribution at a desired equiphase surface; *U. S. Patent* **1969**, 3,476,463.

[32] Rhodes, P. W.; Shealy, D. L. Refractive optical systems for irradiance redistribution of collimated radiation: their design and analysis," *Appl. Opt.* **1980,** 19, 3545-3553.

[33] Rhodes, P. W. Design and analysis of refractive optical systems for irradiance redistribution of collimated radiation; M.S. Thesis, The University of Alabama in Birmingham, **1979**.

[34] Haffnagle, J. A.; Jefferson, C. M. Design and performance of a refractive optical system that converts Gaussian to a flattop beam; *Appl. Opt*. **2000,** 19, 5488-5499.

[35] Jiang, W.; Shealy, D. L.; Martin, J. C. Design and testing of a refractive reshaping system; *Current Developments in Optical Design and Optical Engineering III*, Robert, E.; Fisher; Smith, W. J.; *Proc. SPIE* **1993**, 2000, 64-75.

[36] Jiang, W. Application of a laser beam profile reshaper to enhance performance of holographic projection systems; Ph.D. Dissertation, the University of Alabama at Birmingham, **1993**.

[37] Jiang, W.; Shealy, D.L.; Baker, K.M. Optical design and testing of a holographic projection system; *Diffractive and Holographic Optics Technology*, Cindrich, I; Lee, S. H.; *Proc. SPIE* **1994**, 2152, 244-252.

[38] Dickey, F. M.; Holswade, S. C. Laser Beam Shaping; *Proc. SPIE* **2000,** 4095.

[39] Dickey, F. M.; Holswade, S. C.; Dekker, M. Laser Beam Shaping: Theory and Techniques; New York, **2000**.

[40] Dickey, F. M.; Holswade, S. C.; Shealy, D. L. Laser Beam Shaping II; *Proc. SPIE* **2001,** 4443.

[41] Zhang, Z.; You, Z.; Chu, D. Fundamentals of phase-only liquid crystal on silicon (LCOS) devices; *Light Sci. Appl.* **2014**, 3(10), 213.

[42] Pütsch, O.; Stollenwerk, J.; Loosen, P. Integrated optical design for highly dynamic laser beam shaping with membrane deformable mirrors; *Proc. SPIE* **2017**, 10090, 1009010.

[43] Dickey, F. M.; Weichman, L. S.; Shagam, R. N. Laser beam shaping techniques; *Proc. SPIE* **2000**, 4065.
[44] Dickey, Fred M., and Todd E. Lizotte, eds. *Laser beam shaping applications*. Vol. 1. CRC Press, **2017.**

[45] Efron, U. Spatial light modulators for optical computing and imformation processing; *Sys. Sci.* **1989**, 1, 416.

[46] Huot, N.; Sanner, N.; Audouard, E. Programmable focal spot shaping of amplified femtosecond laser pulses and their application to micromachining; *Proc. SPIE* **2006,** 6400, 6400K.

[47] Scanner, N.; Huot, N.; Audouard, E.; Larat, C.; Huignard, J. Direct ultrafast laser micro-structuring of materials using programmable beam shaping; *Opt. and Lasers Eng.* **2007,** 45, 6, 737-741.

[48] Jesacher, A.; Booth, M. Parallel direct laser writing in three dimensions with spatially dependent aberration correction; *Opt. Exp.* **2010,** 18, 21090.

[49] Kuang, Z.; Perrie, W.; Leach, J.; Sharp, M.; Edwardson, S.; Padgett, M.; Dearden, G.; Watkins, K.; High throughput diffractive multi-beam femtosecond laser processing using a spatial light modulator; *Appl. Surf. Sci.*, **2008,** 255, 2284.

[50] Schulze, E. Real-time holographic 3D imaging based on multiplexing techniques and optoelectronics holograms; *Proc. SPIE* **1987,** 0812, 120–127.

[52] Huang, Y.; Liao, E.; Chen, R.; Wu, S.-T. Liquid-Crystal-on-Silicon for Augmented Reality Displays. *Appl. Sci.* **2018**, 8, 2366.

[53] Gooch, C.H.; Tarry, H.A. The optical properties of twisted nematic liquid crystal structures with twist angles ≤ 90 degrees; *J. Phys. D Appl. Phys.* **1975**, 8, 1575–1584.

[54] Allen, L.; Beijersbergen, M. W.; Spreeuw, R. J. C.; Woerdman, J. P. Orbital angular momentum of light and the transformation of Laguerre-Gaussian laser modes; *Phys. Rev. A* **1992**, 45, 8185.

[55] Mair, A.; Vaziri, A.; Weihs, G.; Zeilinger, A. Entanglement of the orbital angular momentum states of photons; *Nature* **2001,** 412, 313–316.

[56] Leach; Padgett, M.; Barnett, S. M.; Arnold, S. F.; Courtia, J. Measuring the Orbital Angular Momentum of a Single Photon; *Phys. Rev. Lett.* **2002**, 88, 25.

[57] Chen, Q. F.; Shi, B. S; Zhang, Y. S.; Guo, G. C. Entanglement of the orbital angular momentum states of the photon pairs generated in a hot atomic ensemble; *Phys. Rev. A* **2008,** 78, 053810.

[58] Karimi, E.; Santamato, E. Radial coherent and intelligent states of paraxial wave equation; *Opt. Lett.* **2012,** 37, 2484-2486.

[59] Durnin, J.; Miceli, J. J.; Eberly, J. H. Diffraction-free beams; *Phys. Rev. Lett.* **1987,** 59(22), 2611.

[60] J. Durnin, Diffraction-free beams; *J. Opt. Soc. Am. A* **1987,** 4, 651-654.

[61] Lee, H. S.; Stewart, B. W.; Choi, K.; Fenichel, H. Holographic non diverging hollow beam; *Phys. Rev. A.* **1994**, 49(6), 4922-4927.

[62] McGloin, D.; Dholakia, K. Bessel beams: Diffraction in a new light; *Contem. Phys.* **2005**, 46(1), 15-28.

[63] McQueen, C. A.; Arlt, J.; Dholakia, K. An experiment to study a "nondiffracting" light beam; *Am. J. Phys.* **1999,** 67(10), 912-915.

[64] Takaki, Y.; Okada, N. Hologram generation by horizontal scanning of a high-speed spatial light modulator; *Appl. Opt*.**2009,** 48, 3255-3260.

[65] Allen, L.; Padgett, M.; Babiker, M. IV The orbital angular momentum of light; *Progress in Optics* **1999**, 39, 291-372.

[66] Carpentiera, A.V.; Michinel, H.; Salgueiro, J. R. Making optical vortices with computer-generated holograms; **2008,** *Am. J. Phys*. 76, 916.

[67] Arlt, J.; Dholakia, K.; Allen, L.; Padgett, M. The production of multiringed LaguerreGaussian modes by computer-generated holograms; *J. Mod. Opt.* **1998,** 45, 1231-1237.

[68] Cagliero, A.; Gaffoglio, R.; Vita, A. D.; Sacco, B. Modeling OAM Transmission in Waveguides with COMSOL Multiphysics®; *Proceedings of the 2016 COMSOL Conference in Munich* **2016**.

[69] White, A.G.; Smith, C.P.; Heckenberg, N.R.; Rubinsztein-Dunlop, H.; McDuff, R.; Weiss, C.O.; Tamm, C. Interferometric Measurements of Phase Singularities in the Output of a Visible Laser; *J. Mod. Opt.* **1991**, 38(12), 2531-2541.

[70] Chen, X.; Cheng, W.; Xie, M.; Zhao, F. Optical rotational self-assembly at air-water surface by a single vortex beam; *Results Phys.* **2019**, 12, 1172-1176.